

1 **Dear Editor,**

2 We would like to thank you for the time you spent on the manuscript and finding the reviewers.
3 The answers to the review comments were submitted as supplement files on 16 January, 2015,
4 and we have modified the manuscript according to the responses to the reviewer comments (see
5 the responses below, also posted online in the Interactive Discussion). We have also updated
6 the reference list, and corrected a few small typos in the manuscript. We hope that you can
7 consider our manuscript for publication in Atmos. Chem. Phys. and are looking forward to any
8 comments you might have.

9

10 Best regards,

11 **Maryam Dalirian**

12

13 maryam.dalirian@aces.su.se

14 Department of Environmental Science and Analytical Chemistry (ACES)

15 Svante Arrhenius väg 8, SE-11418 Stockholm

16 Sweden

17

18

19 **Reviewer #1**

20 *We thank Reviewer #1 for his/her positive, constructive and detailed comments, which we will*
21 *account for in the revised manuscript. In particular, we would like to thank the reviewer for*
22 *requesting a more detailed treatment of the particle shape and its importance for the CCN*
23 *activation, as we feel that accounting for these comments has improved the manuscript*
24 *considerably. Our point-by-point responses to the issues raised by the reviewer are below.*

25 **Scientific questions:**

26 My only major general comment concerns the agglomeration part of the study. I believe 2
27 important things are missing:

28 1) a discussion of why it is important to consider particle shape in the context of the theoretical
29 frameworks that are discussed. Specifically, what are the physical reasons for using the
30 surface equivalent diameter rather than mobility diameter in each term in Eq. 13?

31 *Particle shape can affect the physical dimensions of the particle in terms of the surface*
32 *available for water vapour to adsorb onto, as well as for the effective curvature determining*
33 *the Kelvin effect (see e.g. Kumar et al., 2011a). This is particularly relevant for the adsorption*
34 *term in Eq. 13 describing the attachment of water molecules on the insoluble silica surface –*
35 *where the available surface is the key parameter to be known for predicting the adsorption*
36 *rates correctly. For the solution term, on the other hand, the total amount of soluble material*
37 *(related to the particle density) is the relevant property to know. In the case of highly non-*
38 *spherical or porous particles the conversion between the electrical mobility (the quantity*
39 *measured with the SMSPS system) and the available surface area or particle volume and*
40 *density is not straight-forward. In our case, we used measurements of particle mass for the pure*
41 *silica agglomerates to complement the information about the mobility of these particles. The*
42 *results suggested that the particles were somewhat in agglomerated shape (fractal dimensions*
43 *of about 2.55 as compared with 3 for spherical particles) and porous. We have added a brief*
44 *discussion on the impacts of particle shape on CCN activation to the revised manuscript.*

45 *In the present paper we used the surface equivalent diameter to account specifically for the*
46 *larger surface area available for the adsorption on the insoluble silica fraction. This has some*
47 *implications for the fitted FHH parameters (see our responses to the next comment and Figs.*
48 *R1-R4). However, as mentioned above, the volume (or mass) equivalent diameter is probably*
49 *more relevant metric for terms describing the solute effects in Eq. 13. In the case where the*
50 *surface and the volume equivalent diameters are very different from each other (e.g. highly*
51 *branched chain-like agglomerates), the two diameters differ from each other (surface*
52 *equivalent diameter is larger than the volume equivalent diameter), and the former is more*
53 *appropriate for describing the adsorption phenomena and the latter the solute effect. For close-*
54 *to-spherical compact agglomerates the surface and volume equivalent diameters are, on the*
55 *other hand, equal to each other and the mobility diameter (but larger than the mass equivalent*
56 *diameter).*

57 *Based on our additional analysis of the particle shape (see the response to the next comment*
58 *and Figs. R1-R4) we conclude that our particles are closer to porous but compact agglomerates*
59 *than chain-like structures – in which case the surface and volume equivalent diameters are*
60 *close to each other and the mobility diameter. In the revised manuscript all the calculations*
61 *applying Eq. 13 have now been made assuming compact agglomerates with surface equivalent*
62 *diameter being roughly equivalent to the volume equivalent and mobility diameters. This does*

63 *not change any of the conclusions of the manuscript but changes some of the absolute numbers*
64 *to come extent, as illustrated in Figs. R1-R4 below.*

65 2) a study of the sensitivity of predicted critical supersaturations to particle shape. Given the
66 sensitivity of predicted critical supersaturations to the FHH adsorption parameters and
67 soluble volume fraction, and the fact that both of these sets of parameters can be difficult to
68 know for ambient particles, is it even necessary to account for particle shape?

69 *Thank you for raising this issue, which prompted us to do a more systematic analysis of the*
70 *influence of the assumed particle shape/porosity on our results. The sensitivity of the results to*
71 *the particle shape and porosity assumption are illustrated for pure silica and the mixed*
72 *particles in Figs. R1-R4 below. In these figures we have tested two limiting assumptions about*
73 *the particle shape, using the information on the mobility diameter d_b (available from the SMPS*
74 *for both the pure silica and the mixed particles) and the particle mass and mass equivalent*
75 *diameter d_{me} (available from the APM measurements for pure silica). With this amount of*
76 *information at hand (i.e. no direct measurement of the particle density), the two limiting*
77 *assumptions for the pure silica are:*

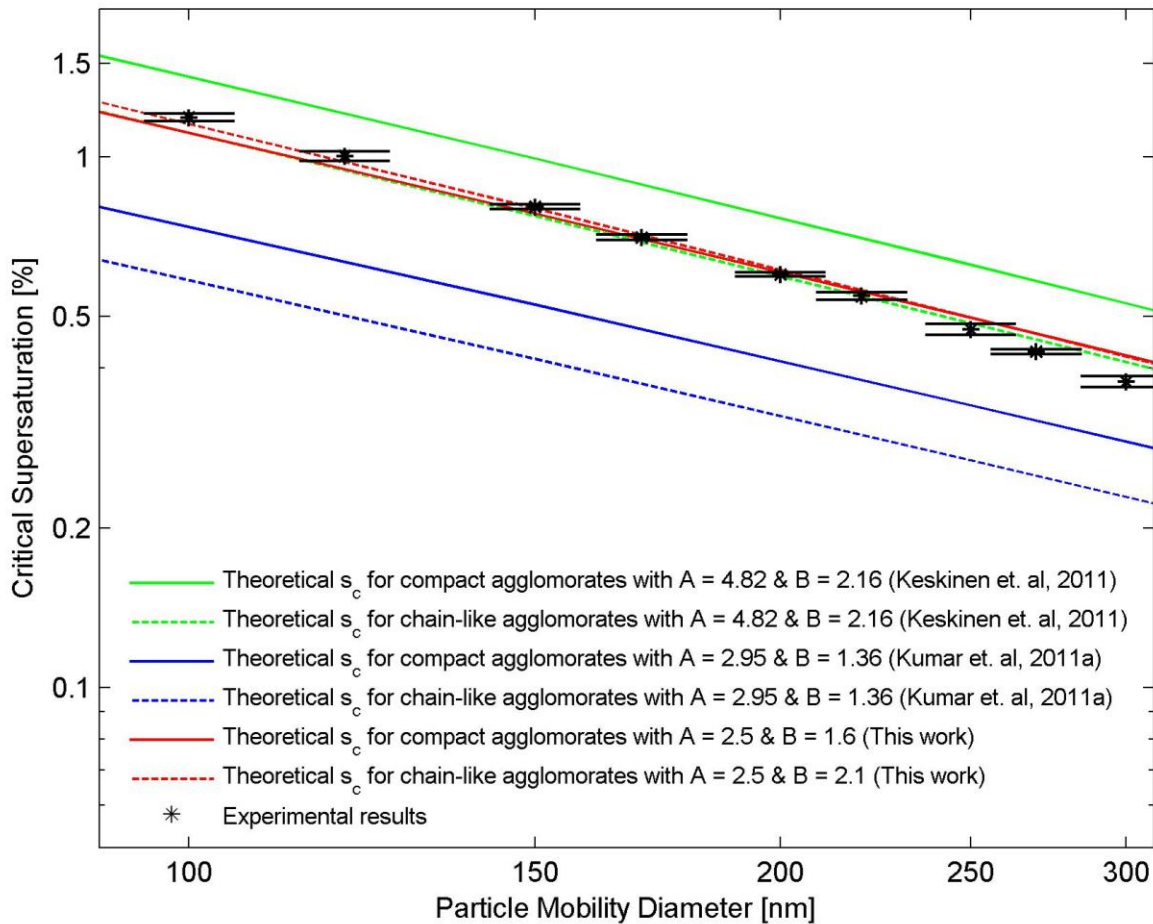
78 1) *Assuming the silica particles are compact agglomerates having nearly spherical shape*
79 *but internal voids. In this case the mobility (d_b) and volume equivalent diameters (d_{ve})*
80 *are approximately the same and also equal to surface equivalent diameter (d_{se}), but*
81 *larger than the mass equivalent diameter (d_{me}) i.e. $d_b = d_{ve} = d_{se} > d_{me}$. The particle*
82 *density is in this case lower than the pure silica material density (DeCarlo et al., 2004),*
83 *but equal to the effective density.*

84 2) *Considering the silica particles as chain-like agglomerates with no internal voids, for*
85 *which mass and volume equivalent diameters are equal (DeCarlo et al., 2004), but*
86 *smaller than surface equivalent and mobility diameters, i.e. $d_{ve} = d_{me} < d_{se}$ and d_b . In*
87 *this case the particle density would be the same as the pure silica material density but*
88 *higher than the effective density.*

89 *The predicted critical supersaturations vs. mobility diameters resulting from analysing the*
90 *silica data with these two assumptions are presented in Fig. R1, using the literature values for*
91 *the FHH adsorption parameters A_{FHH} and B_{FHH} (Keskinen et al., 2011; Kumar et al., 2011a),*
92 *or fitting them to our data separately for each assumption – using the surface equivalent*
93 *diameter d_{se} as the dry diameter in Eq. 12. It can be seen that while the assumption on the shape*
94 *does not have a drastic effect on the results, the “compact agglomerates” assumption yields*
95 *higher critical supersaturations for given A_{FHH} and B_{FHH} values as compared with the “chain-*
96 *like agglomerates” assumption. For the case of fitted A_{FHH} and B_{FHH} , on the other hand, the*
97 *assumed shape does not influence the value determined for A_{FHH} , while the B_{FHH} value is*
98 *affected rather significantly. We have discussed this sensitivity of the results to the assumption*
99 *of the silica particle shape in the revised manuscript.*

100 *The fractal dimension D_f determined from the data provides further insight on the sphericity of*
101 *the silica particles (DeCarlo et al., 2004; Boldridge, 2010; Keskinen et al., 2011), for perfect*
102 *spheres $D_f = 3$ and for line-like structures $D_f = 1$. The D_f values determined from our data were*
103 *of the order of 2.54-2.55, thus suggesting closer to spherical rather than rod- or chain-like*
104 *structures. We therefore expect the silica particles to be better represented by the “compact*
105 *agglomerates” assumption above, and have thus used this assumption for interpreting the data*

106 throughout the revised manuscript (i.e. just present the predictions corresponding to the solid
 107 lines in the revised manuscript).

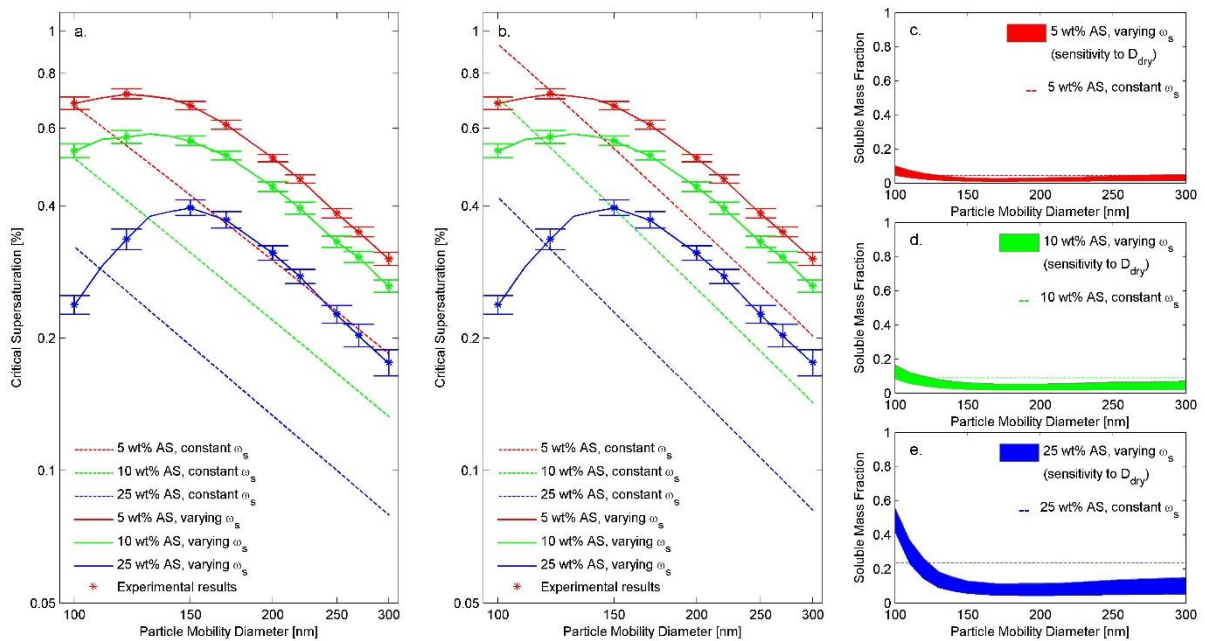


108
 109 Fig. R1: Critical supersaturations against the critical mobility diameter of pure silica particles with
 110 different FHH adsorption isotherms and assuming either compact but porous agglomerates (solid lines)
 111 or chain-like agglomerates (dashed lines).

112 As mentioned above, the mass analysis results were only available for the pure silica particles.
 113 When analysing the CCN activation data for the mixed particles, we assumed that the effective
 114 density of the silica in the mixed particles was similar to the effective density of the pure silica
 115 particles. The physical meaning of this assumption in the “compact agglomerates” assumption
 116 would be that the silica present in the mixed particles would contain the same volume of voids
 117 per unit silica mass as the pure particles. Furthermore, when calculating the critical
 118 supersaturations using Eq. 13 the adsorption term was calculated using the surface equivalent
 119 diameter d_{se} as d_{dry} and the solubility term using the volume equivalent diameter d_{ve} as d_{dry} . The
 120 sensitivity of the critical supersaturation predictions and the corresponding distribution of the
 121 soluble material calculated this way are presented in Figs. R2-R4. For the mixtures with
 122 ammonium sulphate (Fig. R2) the assumption about the particle shape does not affect the
 123 results significantly. For the mixtures with sucrose, a larger sensitivity is observed – the “chain-
 124 like agglomerates” assumption predicting considerably higher critical supersaturations than
 125 the “compact agglomerates” assumption for a given constant soluble fraction (Figs. R3a-b).
 126 In accordance with this, the size-dependent fitted soluble fractions (Figs. R3c-e) assuming

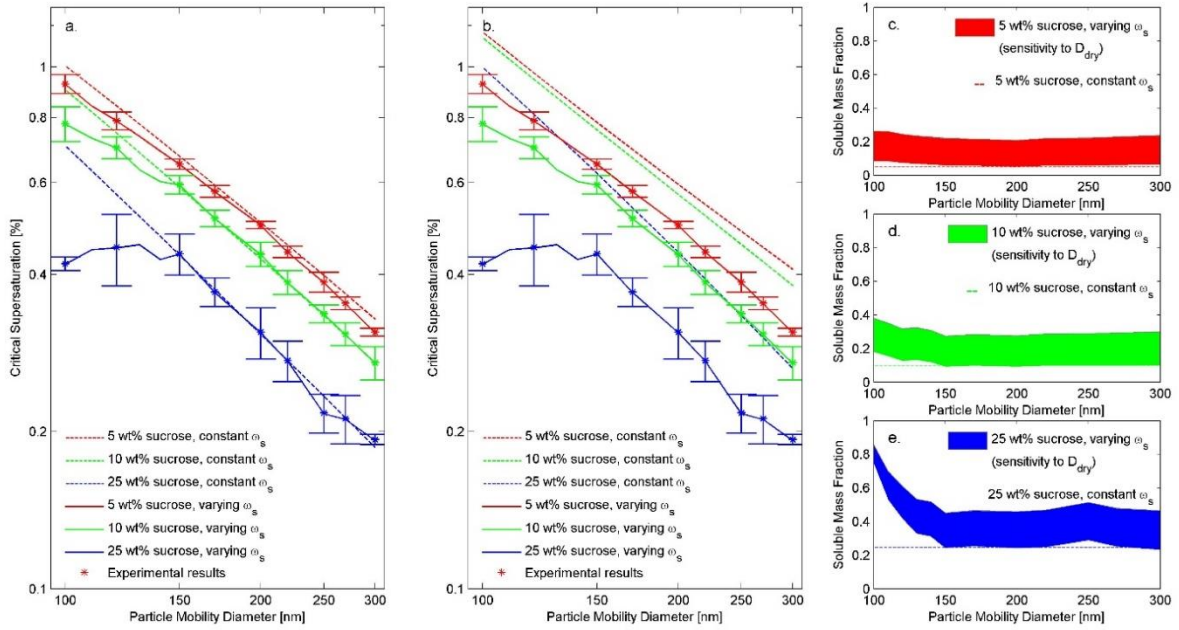
127 compact agglomerates are lower than the corresponding values for the chain-like assumption.
 128 In fact, it is notable that the soluble fractions fitted for the chain-like assumption are
 129 consistently higher than the soluble fraction in the atomized solution – which is probably not
 130 realistic. This further suggests that the “compact agglomerate” assumption is probably more
 131 reasonable in the case of the mixed particles containing silica and sucrose. The corresponding
 132 results for the mixed silica + BSA particles are shown in Fig. R4. First, it should be noted that
 133 the different mixture compositions lie relatively close to each other in terms of their critical
 134 supersaturations – making it difficult to constrain the soluble contents of these particles.
 135 However, it seems clear that at the small particle sizes (< 150 nm) the particle population is
 136 dominated by pure BSA particles. At sizes between 150 and 250 nm, on the other hand,
 137 extremely low BSA-content is required to reproduce the observed critical supersaturations.
 138 This is of course also visible in Fig. 8c of the present paper, where the mixtures with low BSA-
 139 content seem to activate at even higher supersaturations than pure silica. We do not know the
 140 exact reason for this, but the effect of BSA on silica particle structure (e.g. density etc.) could
 141 be speculated upon.

142 Given these overall results on the sensitivity to the shape assumption, we have applied the
 143 “compact agglomerate” assumption (i.e. $d_b = d_{ve} = d_{se}$) in all the theoretical calculations (in
 144 particular Eqs. 12-13) and the corresponding figures of the revised manuscript.



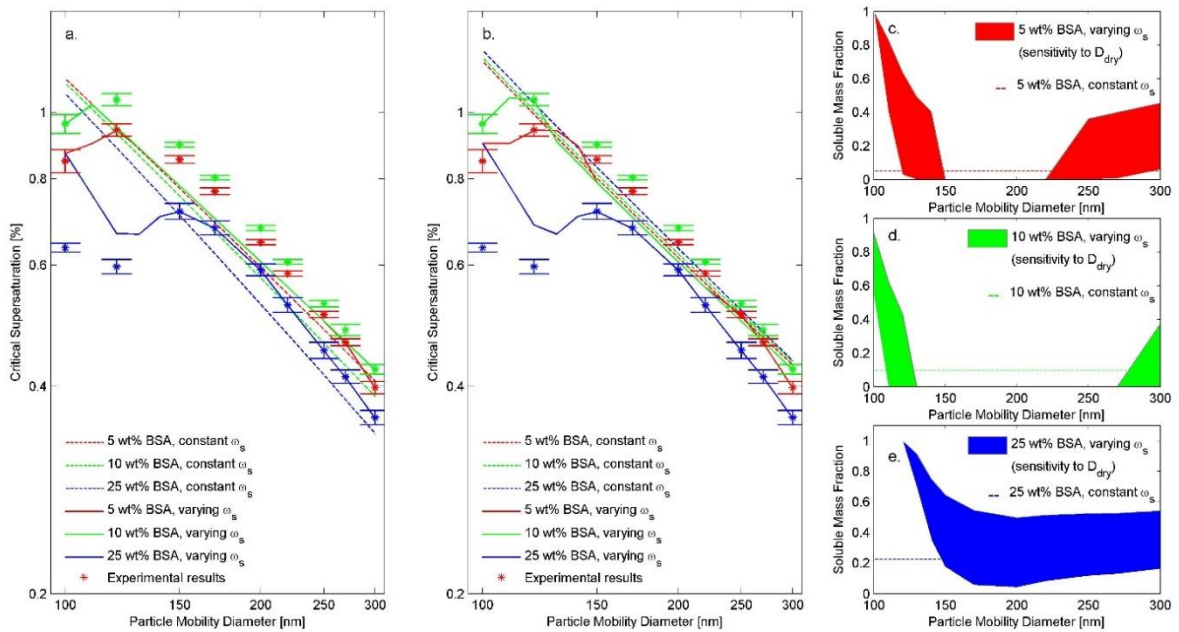
145
 146 Fig. R2: Experimental and theoretical critical supersaturations for mixed silica + (NH₄)₂SO₄ (AS)
 147 particles vs. particle mobility diameters using different assumptions of particle shape and porosity.
 148 a) Critical supersaturations calculated assuming “compact agglomerates” for constant and varying ω_s .
 149 b) Critical supersaturations calculated assuming “chain-like agglomerates” for constant and varying
 150 ω_s . c-e) The sensitivity of the distribution of soluble material to these two assumptions. The upper limit
 151 corresponds to the “chain-like agglomerates” assumption and the lower limit to the “compact
 152 agglomerates” assumption.

153



154

155 *Fig. R3: Experimental and theoretical critical supersaturations for mixed silica + sucrose particles vs.*
 156 *particle mobility diameters using different assumptions of particle shape and porosity. a) Critical*
 157 *supersaturations calculated assuming “compact agglomerates” for constant and varying ω_s . b) Critical*
 158 *supersaturations calculated assuming “chain-like agglomerates” for constant and varying ω_s . c-e) The*
 159 *sensitivity of the distribution of soluble material to these two assumptions. The upper limit corresponds*
 160 *to the “chain-like agglomerates” assumption and the lower limit to the “compact agglomerates”*
 161 *assumption.*



162

163 *Fig. R4: Experimental and theoretical critical supersaturations for mixed silica + BSA particles vs.*
 164 *particle mobility diameters using different assumptions of particle shape and porosity. a) Critical*
 165 *supersaturations calculated assuming “compact agglomerates” for constant and varying ω_s . b) Critical*
 166 *supersaturations calculated assuming “chain-like agglomerates” for constant and varying ω_s . c-e) The*
 167 *sensitivity of the distribution of soluble material to these two assumptions. The upper limit corresponds*
 168 *to the “chain-like agglomerates” assumption and the lower limit to the “compact agglomerates”*
 169 *assumption.*

170 **Specific comments**

171 P 23174, L18 - It seems the mass measurements were only performed for pure silica particles.
172 What surface equivalent diameters were used for the mixed particles?

173 *The reviewer is correct – the mass measurements were only conducted for pure silica. In the*
174 *present manuscript the surface equivalent diameters used were in fact calculated using the*
175 *effective density of silica determined from the mass measurements (and be equivalent to the*
176 *pure silica particle density, corresponding to the “chain-like agglomerate” assumption) and*
177 *the material density of the soluble species. However, as clarified above, in the revised*
178 *manuscript we have rather used the silica particle density determined using the “compact*
179 *agglomerate” assumption and assuming that $d_b = d_{ve} = d_{se}$.*

180 P 23174, L 24 - Were the contributions of the smaller soluble particle mode subtracted from
181 both the CCN and CN measurements? How were the contributions of the smaller completely
182 soluble particles to CCN concentrations determined? From theory?

183 *First, the contribution of pure soluble particles to the total number of CN for each size were*
184 *estimated by fitting two log-normal modes to the size distributions such as those shown in Fig.*
185 *2. These were then subtracted from the CN data for each size to yield an estimate of the total*
186 *numbers of mixed CN. Second, using the CCN/CN ratios of the pure soluble particles (shown*
187 *for 120 nm in Fig. 4) we could estimate the number of CCN originating from pure CN at each*
188 *mobility diameter and supersaturation. Subtracting this from the total number of CCN, we*
189 *could yield an estimate for the CCN/CN ratio for the mixed particles, shown in Fig. 8. We have*
190 *clarified this procedure in the revised manuscript.*

191 P 23175, L 25 - Confusing statement. The AFHH coefficient derived in this work is similar to
192 that reported by Kumar (2011a) but the BFHH coefficients are quite different, which I guess is
193 why the results agree better with the Keskinen (2011) curve than Kumar (2001a) curve in Fig.
194 6?

195 *Given the results shown in Fig. R1, the “compact agglomerate” assumption actually makes the*
196 *results for fitted FHH-parameters relatively close to those by Kumar et al. (2011a). We have*
197 *revised this statement accordingly.*

198 P 23175, L 25 “although the AFHH and BFHH values are close to those reported by Kumar et
199 al. (2011a)” → ” B_{FHH} value in this study is closer to that reported by Keskinen et al. (2011)”

200 *Given the revised treatment of the pure silica data, both fitted values are now actually closer*
201 *to those reported by Kumar et al. (2011a). We have modified the revised manuscript*
202 *accordingly.*

203 P 23175, L 26 – It’s concluded that these data are not sufficient to uniquely constrain the FHH
204 adsorption parameters. What would be sufficient data? Given the complexity of atmospheric
205 aerosols is it reasonable to expect useful FHH adsorption parameters could be obtained for
206 modelling more complex systems?

207 *This is an interesting question, which we do not have a definite answer for. Based on our results*
208 *it can be seen that in particular parameter A_{FHH} , describing the interactions of the first*
209 *monolayer and the adsorbate surface, seems to be difficult to constrain based on the CCN*
210 *activation data (see Fig. 6 in the paper). This is perhaps not surprising as at the point of*
211 *activation the rapid condensation of water might relatively soon destroy the information of the*

212 *very first steps of the adsorption / monolayer formation. For the parameter B_{FHH} , on the other*
213 *hand, the fits seem to reproduce relatively robust values. CCN activation measurements are*
214 *probably not the best approach for yielding accurate data of the physical phenomena behind*
215 *the adsorption parameters – as a lot of information has already been lost at the point where*
216 *the CCN are activated and detected – but should be rather regarded as a valuable source of*
217 *information on the processes limiting atmospheric cloud droplet formation. We have added a*
218 *brief discussion on this to the revised manuscript.*

219 P 23176, L6 - How pure? Need to be more specific since it is not mentioned in the experimental
220 methods section.

221 *De-ionized water with the resistivity $> 10 M\Omega\text{-cm}$ and TOC concentration $< 5\text{ppb}$ was used in*
222 *our experiments. We have added this information to the revised manuscript.*

223 P 23177, L14 - The structure idea could be tested by exploring the sensitivity of critical
224 supersaturation to particle shape as mentioned above. E.g. Is the range of theoretical predictions
225 of critical supersaturation for realistic shape factors comparable to the differences in critical
226 supersaturation observed in Fig. 8c.

227
228 *This is a good point. As discussed above, the results do seem to support the idea that the BSA*
229 *particles affects the stability of the silica particles.*

230
231 P 23197, Fig 9 - (and Figs. 10 and 11) Recommend keeping the same colour code as Figure 8,
232 red – 5

233
234 *Thank you for pointing this out. The colour codes for particles corresponding to the 5 & 10 %*
235 *solute fractions have been exchanged in the Figs. 9, 10 & 11 of the revised manuscript.*

236
237 **Technical comments**

238 P 23171, L18 - Typo in the equation for ϵ_s

239
240 *Thank you for pointing this out. We have replaced $\epsilon = 1 - \epsilon$ with $\epsilon_s = 1 - \epsilon_i$ in the revised manuscript.*

241 P 23177, L24 and 28 - Typos in ω and ϵ

242
243 *Thank you for pointing this out. We have replaced ω_{sS} with ω_s and ϵ_{sS} with ϵ_s in the revised*
244 *manuscript.*

245

246

247

248 **Reviewer #2**

249
250 *We thank Reviewer #2 for his/her positive, constructive and detailed comments, which we will*
251 *account for in the revised manuscript. Our point-by-point responses to the issues raised by the*
252 *reviewer are below.*

253 **Scientific questions:**

254 I have reservations to word “coating” used in this study, simply I do not see clear experimental
255 evidence, to believe that authors are able to coat silica by mixing it with salt, sugar or protein
256 in water, without any special treatment – high temperatures, oxidation or similar. Even though
257 the authors claim they used hydrophilic fumed silica.

258 *We agree that the term “coating” is not an accurate description of our mixed particles. We*
259 *have modified the revised manuscript accordingly, using the term “mixture” instead of*
260 *“coating”.*

261 **Specific comments**

262 Page 6, mid paragraph about CCNc, it would be good to mention what sheath and sample flows
263 of CCNc were used during the experiment.

264 *We have modified the revised manuscript by adding the following text to the the paragraph in*
265 *question: “Humidified sheath flow ($454 \text{ cm}^3 \text{ min}^{-1}$) surrounds the sample flow ($45.4 \text{ cm}^3 \text{ min}^{-1}$)*
266 *in the CCN column to hold it in the centre of the column in the region of maximum*
267 *supersaturation. The ratio of the flows was thus 1 part of sample air to 10 parts of sheath air*
268 *and the total flowrate was $500 \text{ cm}^3 \text{ min}^{-1}$. “*

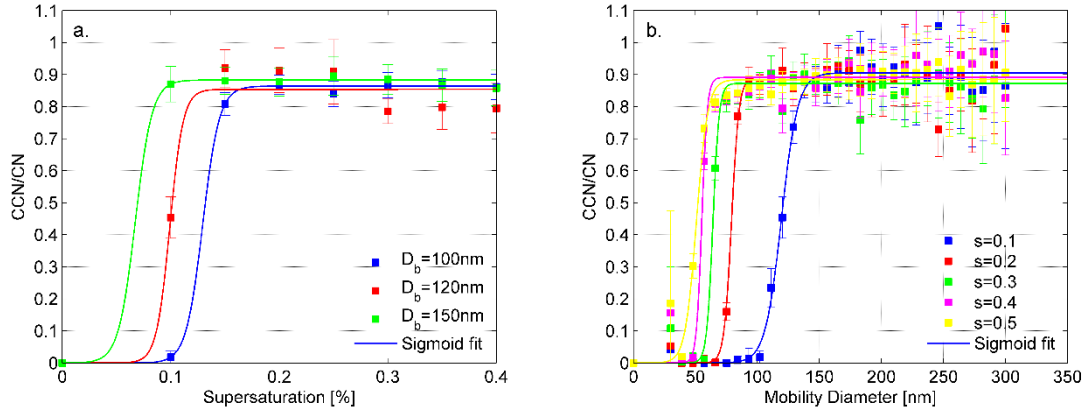
269 Page 7 eq. 3, is not it enough to make reference only to original source? Why to reference to
270 four manuscripts? Similarly through the whole manuscript.

271 *This is a good point. We have modified the revised manuscript accordingly.*

272 Page 13 starting line 361, authors discuss the use of previously reported kappa parameter from
273 literature, listed in Table 1. Why they do not use their own, as showed in Fig.7? Or were the
274 experimentally obtained kappa values exactly the same as reported in literature? Would be
275 beneficial to see activation curves as a function of mobility diameter for pure compounds, since
276 in Fig 8 the activation curves for 150 nm do not reach unity in activation, especially in the case
277 of ammonium sulphate which is used for CCNc calibration.

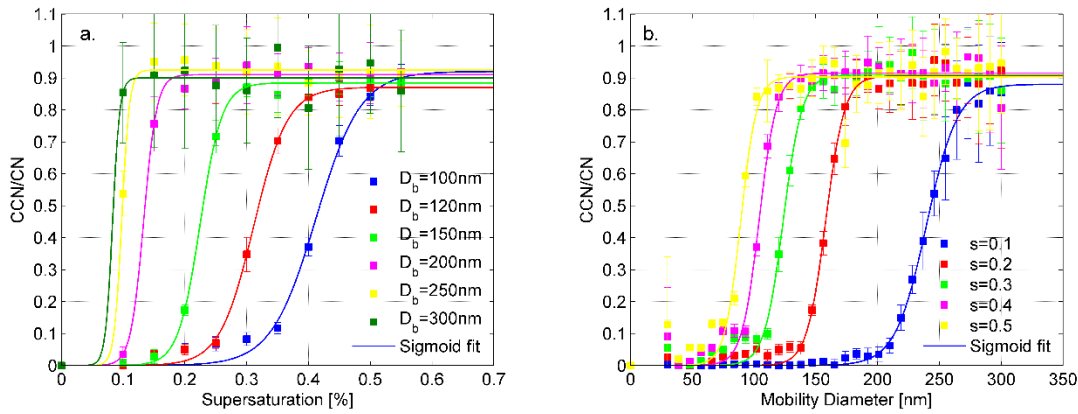
278 *We used the literature values for κ of ammonium sulphate (AS) and sucrose to demonstrate the*
279 *good agreement between our results and previous work on pure component activation. The κ*
280 *values fitted for AS and sucrose using our experimental data would be 0.78 and 0.08. We have*
281 *added this information to the revised manuscript. Here we should probably also clarify that all*
282 *the activation curves that were used in further analysis were normalized, using a correction*
283 *factor derived from the ammonium sulphate experiments, assuming that AS activation*
284 *probability reaches unity at high supersaturations. Figs. R1-R3 show the unnormalized data on*
285 *the activation curves as a function of diameter and supersaturation, as requested by the*
286 *reviewer. We have clarified the normalization procedure in the revised manuscript and add*
287 *also the normalized curves (which were used in the analysis) to Fig. 8.*

288



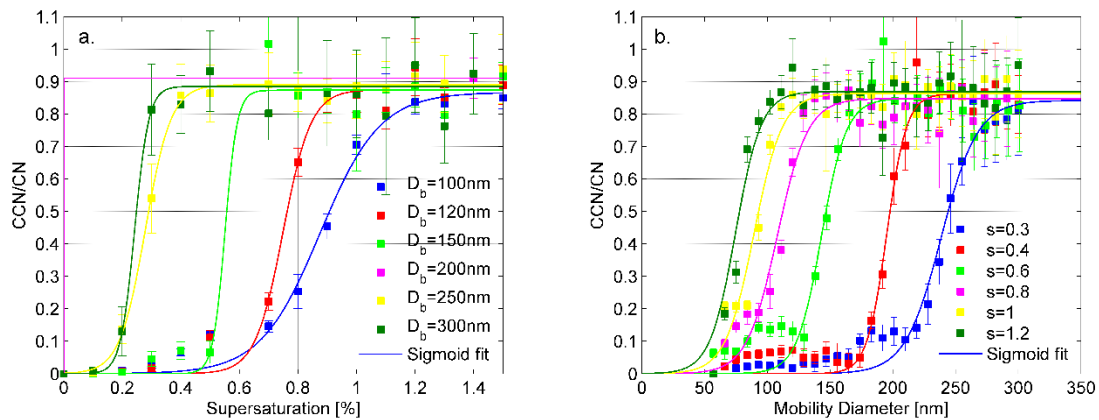
289 *Fig. R1: a) The average activation ratio vs. supersaturation for pure $(\text{NH}_4)_2\text{SO}_4$ particles in*
290 *different mobility diameters. b) The average activation ratio vs. mobility diameter for pure*
291 *$(\text{NH}_4)_2\text{SO}_4$ particles in different supersaturations.*

292



293 *Fig. R2: a) The average activation ratio vs. supersaturation for pure sucrose particles in*
294 *different mobility diameters. b) The average activation ratio vs. mobility diameter for pure*
295 *sucrose particles in different supersaturations.*

296



297 *Fig. R3: a) The average activation ratio vs. supersaturation for pure BSA particles in*
298 *different mobility diameters. b) The average activation ratio vs. mobility diameter for pure*
299 *BSA particles in different supersaturations.*

300

301 Page 15 line 411, I see this part as very problematic. In Kumar et al (2011b) you can find that
302 they were using several samples of real mineral dust collected in several locations. I have no
303 doubts that their samples undergo certain natural process of aging and use of shell-core model
304 in their case is appropriate. However, this is not the case of this study, making water
305 solution/dispersion of fumed silica and ammonium sulphate (max 25% mass fraction) will not
306 lead to any coating. If authors have different opinion I would like to see any proof of that. For
307 example preparing the dispersion, in the same way as in this work, of aquadac (colloidal
308 graphite) and 70 % mass fraction of AS leads only to about 10% of coated particles, the rest is
309 externally mixed. In the case of BC containing particles you can find out the shell thickness
310 using single particle soot photometer (SP2-DMT, CO, USA), in the case of this study I
311 understand that such a kind of analysis is very difficult. On the other hand the presence of
312 externally mixed particles should be visible from activation spectra (CCN/CN vs D_p) as
313 activated fraction plateaus at a value that is different from unity. I would recommend authors
314 broader discussion with justification for usage of shell-core model or simply omit this part. I
315 am not sure if sucrose and BSA are doing better job in coating than AS.

316 *We fully agree that our mixed particles are not exactly coated, and, as also stated above, we*
317 *will removed the term “coating” when referring to our mixed particles throughout the text in*
318 *the revised manuscript. Indeed, there is a wide range of compositions present at a given size*
319 *range, as also shown in our Figs. 8-11 for all the soluble compounds. However, we also agree*
320 *that if two distinct aerosol populations (e.g. “mixed” and “pure” particles) we present as a*
321 *simple external mixture we should see two plateaus in the CCN activation curve – which we*
322 *don’t. Instead, we see a relatively shallow CCN/CN vs. supersaturation curve (see Fig. 8),*
323 *supporting the hypothesis of a continuous distribution of soluble vs. insoluble volume/mass*
324 *fractions in the particles – as also indicated by the results shown in Figs. 9-12 in the*
325 *manuscript. We tried to highlight this in the sentence describing these figures beginning with:*
326 *“The small contribution of the adsorption term to the theoretical predictions combined with the*
327 *shallow activation ratio curves (see Fig. 8) suggest that the reason for the apparent discrepancy*
328 *between the theoretical and the observed critical supersaturations is a non-constant*
329 *distribution of the soluble material with varying particle size.” Also, while the model by Kumar*
330 *et al. (2011b) was indeed originally introduced for fresh dust coated by a layer of soluble salt*
331 *after aging, which is not the case for our experiments, it is currently the only readily applicable*
332 *theoretical formation, and we believe it does give a reasonable estimate on the potential*
333 *importance of the adsorption as compared with the bulk solubility of the mixed particles. We*
334 *have clarified this and discuss the limitations of our approach more thoroughly in the revised*
335 *manuscript.*

336 Page 17 sentence starting on line 498: Similarly as the previous comment, “Our mixed particles
337 : : : representing an aerosol population with various degree of aging in atmosphere.” I have hard
338 time to agree with such conclusion. I would encourage the authors to provide any arguments to
339 support use of word “aging”. Fig 9-11 shows directly disagreement with shell-core model.

340 *We agree with you. We have removed this sentence and modified the revised manuscript*
341 *accordingly.*

342 Fig. 3 would be nice to see some statistical measure of the fits, e.g. coefficient of determination.

343 *We have added the R^2 values for the fits to Fig. 3 in the revised manuscript (see below).*

344 *In Fig. 3a: $R^2=0.992$*

345 *In Fig. 3b: $R^2=0.978$ & 0.997*

346 *In Fig. 3c: $R^2=0.991$*

347

348

349 **CCN activation of fumed silica aerosols mixed with soluble**
350 **pollutants**

351 **M. Dalirian¹, H. Keskinen^{2,3}, L. Ahlm¹, A. Ylisirniö², S. Romakkaniemi^{2,5}, A.**
352 **Laaksonen^{2,4}, A. Virtanen² and I. Riipinen¹**

353 [1] {Department of Applied Environmental Science (ITM) and the Bolin Centre for Climate
354 research, Stockholm University, Stockholm, Sweden }

355 [2] {Department of Applied Physics, University of Eastern Finland, Kuopio, Finland }

356 [3] {Department of Physics, University of Helsinki, Helsinki, Finland }

357 [4] {Finnish Meteorological Institute, Helsinki, Finland }

358 [5] {Finnish Meteorological Institute, Kuopio, Finland }

359

360 Correspondence to: M. Dalirian (maryam.dalirian@itmmaces.su.se)

361

362 **Abstract:**

363 Particle-water interactions of completely soluble or insoluble particles are fairly well
364 understood but less is known of aerosols consisting of mixtures of soluble and insoluble
365 components. In this study, laboratory measurements were performed to investigate cloud
366 condensation nuclei (CCN) activity of silica particles ~~coated-mixed~~ with ammonium sulphate
367 (a salt), sucrose (a sugar) and bovine serum albumin known as BSA (a protein). ~~In addition,~~
368 ~~†The agglomerated structure of the silica particles was investigated by estimating the surface~~
369 ~~equivalent diameter based on using~~ measurements with a Differential Mobility Analyzer (DMA)
370 and an Aerosol Particle Mass Analyzer (APM). ~~Based on these data, the particles were assumed~~
371 ~~to be compact agglomerates when studying their CCN activation capabilities. By using the~~
372 ~~surface equivalent diameter the non-sphericity of the particles containing silica was accounted~~
373 ~~for when estimating CCN activation.~~ Furthermore, ~~characterizing the~~ critical supersaturations
374 of particles consisting of pure ~~and mixed~~ soluble ~~on and~~ insoluble compounds ~~were explored~~
375 using existing ~~theoretical~~ frameworks. ~~These results~~ showed that the CCN activation of single
376 component particles was in good agreement with Köhler and adsorption theory based models
377 when the agglomerated structure was accounted for. For mixed particles the CCN activation

378 was governed by the soluble components, and the soluble fraction varied considerably with
379 particle size for our wet-generated aerosols. Our results confirm the hypothesis that knowing
380 the soluble fraction is the key parameter needed for describing the CCN activation of mixed
381 aerosols, and highlight the importance of controlled coating techniques for acquiring a detailed
382 understanding of the CCN activation of atmospheric insoluble particles mixed with soluble
383 pollutants.

384

385 **Keywords:** Silica, CCN activation, Mixture aerosols, ~~Soluble coatings~~

386 **1 Introduction**

387 The atmosphere of the Earth is composed of gases and suspended liquid and solid aerosol
388 particles of different size, shape, and chemical composition. Atmospheric aerosols have several
389 important impacts on the environment. First, at high concentrations in urban areas, they are a
390 health hazard to the respiratory system causing millions of premature deaths every year (~~Jacob,~~
391 ~~1999; Mackay and Mensah, 2004; Pope and Dockery, 2006; Pope et al., 2009; Tranfield and~~
392 ~~Walker, 2012)~~(~~Mackay and Mensah, 2004; Pope and Dockery, 2006; Pope et al., 2009~~). Second,
393 they scatter and absorb solar and thermal radiation and thereby directly influence the heat
394 balance of the Earth and thus the climate (~~Twomey, 1974; McCormick and Ludwig, 1976; Jacob,~~
395 ~~1999; Haywood and Boucher, 2000; Ramanathan et al., 2001; Lohmann and Feichter, 2005)~~
396 (~~McCormick and Ludwig, 1976; Haywood and Boucher, 2000; Ramanathan et al., 2001~~). Third,
397 they act as cloud condensation nuclei (CCN) and ice nuclei (IN). Hence, they alter the
398 microphysical properties of clouds and thereby indirectly affect the climate (~~Twomey, 1974;~~
399 ~~Twomey et al., 1984; Albrecht, 1989; Jacob, 1999; Haywood and Boucher, 2000; Lohmann and~~
400 ~~Feichter, 2005; Mefiggans et al., 2006)~~ (~~Twomey, 1974; Albrecht, 1989; Lohmann and~~
401 ~~Feichter, 2005~~). Fourth, atmospheric surface and condensed-phase chemistry can occur in the
402 aerosol phase (~~Jacob, 1999)~~(~~Ravishankara, 1997; Seinfeld and Pandis, 2006~~).

403 Aerosol-cloud interactions represent the largest uncertainty in predictions of the future
404 climate (~~IPCC, 2013)~~(~~Carslaw et al., 2013; IPCC, 2013; Lee et al., 2013~~). To reduce this
405 uncertainty we need to improve our understanding of the activation of aerosol particles to cloud
406 droplets. In general, the ability of aerosol particles to act as CCN depends on their composition,
407 size and structure (Kumar et al., 2011a). Besides soluble aerosol particles, insoluble particles
408 like soot, mineral dust, and silica can act as CCN – particularly if they are coated with
409 hygroscopic material (Kumar et al., 2009).

410 During atmospheric transport and aging, originally insoluble particles may acquire
411 soluble species like $(\text{NH}_4)_2\text{SO}_4$ (ammonium sulphate) on their surfaces (Levin et al., 1996). In
412 such cases, the threshold supersaturation of cloud droplet activation substantially decreases
413 when water adsorbs onto the slightly soluble particles giving rise to the process of adsorption
414 activation (Saathoff et al., 2003; Hings et al., 2008). Thus, the presence of soluble species on
415 insoluble particle surfaces can enhance water-particle interactions and CCN activity of the
416 particles. Several recent studies have focused on the CCN activation of insoluble and mixed
417 soluble-insoluble particles, leading to the development of new theoretical frameworks for
418 describing the relevant phenomena. The developed theories are often based on multilayer

419 adsorption models and account for the curvature effects of the particles. One of these theories
420 introduced by Sorjamaa and Laaksonen (2007) combined FHH (Frenkel, Halsey and Hill)
421 adsorption isotherms and traditional Köhler theory to describe the equilibrium growth of
422 insoluble particles. Sorjamaa and Laaksonen (2007) showed that adsorption could help wettable
423 insoluble compounds to activate in the atmosphere. Thereafter, Kumar et al. (2009) developed
424 a cloud droplet formation parameterization where the CCN constitute an external mixture of
425 soluble aerosol, that follows Köhler theory, and insoluble aerosol, that follows FHH adsorption
426 activation theory (FHH-AT). They tested the new parameterization by comparing it to a
427 numerical cloud model and found a good agreement between the parameterization and the
428 model. Later Kumar et al. (2011a) reported laboratory measurements of CCN activity and
429 droplet activation kinetics of aerosols dry generated from clays, calcite, quartz, silica and desert
430 soil samples. They used FHH adsorption activation theory for describing fresh dust CCN
431 activity and found that the adsorption activation theory describes fresh dust CCN activity better
432 than Köhler theory. Afterward, Kumar et al. (2011b) studied particle size distributions, CCN
433 activity, and droplet activation kinetics of wet generated aerosols from mineral particles and
434 introduced a new framework of CCN activation of dust containing a soluble salt fraction, based
435 on a combination of the traditional Köhler and FHH adsorption theories. Henning et al. (2010)
436 on the other hand, studied agglomerated soot particles coated with levoglucosan and ammonium
437 sulphate, and concluded that traditional Köhler theory was sufficient to describe the CCN
438 activation of these mixed particles – as long as the amount of soluble material in the particles
439 was known (see also Stratmann et al., 2010). Despite these pioneering studies, CCN activation
440 measurements of partly insoluble particles containing a soluble fraction are still scarce.

441 Combustion processes result in emissions of different types of anthropogenic
442 nanoparticles. Flame-made (fumed) silica (SiO_2) particles, mainly produced in flame reactors,
443 are among these kind of particle types (Scheckman et al., 2009). Recently, fumed silica particles
444 have been taken into consideration due to their industrial importance (Scheckman et al., 2009;
445 Keskinen et al., 2011). In this study we use fumed silica particles as an experimental model to
446 investigate the CCN activation of the insoluble and partly soluble particles and the applicability
447 of the current theoretical frameworks developed to describe this phenomenon. Furthermore,
448 since the presented theories generally assume that the insoluble particles are spherical, the
449 agglomerated structure of the silica particles could cause uncertainties in the CCN activation
450 parameterizations. Taking into account the shape characterization of aggregated silica particles
451 may overcome these uncertainties. Different studies have recently focused on parameterizing

452 the structure of aggregated particles, especially silica agglomerates (Fuchs, 1964; DeCarlo et
453 al., 2004; Virtanen et al., 2004; Biskos et al., 2006; Scheckman et al., 2009).

454 The main aims of this study are: 1) measuring the CCN activity of pure and mixed
455 soluble-insoluble particles, 2) analysing and comparing the experimental results with
456 theoretical calculations using the existing frameworks and 3) connecting the mass analysis and
457 shape characterization of agglomerated silica particles to the existing theoretical frameworks to
458 gain a better understanding of the structure effects of these particles. Laboratory measurements
459 on the particle size distribution, mass, morphology and CCN activation of insoluble fumed
460 silica mixed with different amounts of soluble materials ~~were~~have been conducted.
461 Furthermore, the experimental CCN activity results ~~were~~are compared to theoretical
462 calculations using the framework introduced by Kumar et al. (2011b), and the distribution of
463 soluble material on wet-generated particle populations ~~is~~was discussed.

464

465 **2 Experimental setup**

466 Pure soluble or insoluble and mixed soluble-insoluble particles were generated and analysed in
467 this study. The investigated mixed particles consisted of fumed silica (Degussa, Aerosil-90) as
468 the insoluble part and three different hygroscopic components as the soluble part. The first
469 hygroscopic component was ammonium sulphate which is a water-soluble inorganic salt with
470 high hygroscopicity (Table 1); the second one was sucrose which is a sugar, i.e. a water-soluble
471 organic; the third one was bovine serum albumin (BSA) which is a large water-soluble protein
472 with molecular dimensions of approximately $4 \times 4 \times 14$ nm (Sugio et al., 1999; Jeyachandran
473 et al., 2010) . The SiO₂ used in the experiments was hydrophilic fumed silica, with a specific
474 surface area of 90 m²/g and purity of $\geq 99.8\%$ from Evonik Industries. Ammonium sulphate
475 and BSA were purchased from Sigma-Aldrich, and sucrose was purchased from VWR
476 International BVBA. All chemicals had purities higher than 99%.

477 Figure 1 shows a schematic of the experimental setup used in this study. Pure silica and
478 pure soluble particles as well as mixed particles made of silica and soluble species were
479 produced using the atomization-drying method described in Keskinen et al. (2011). Particles
480 were generated by an aerosol generator (Model 3076, TSI Inc., USA) after dissolving materials
481 in de-ionized water (Model Maxima LS., USF Elga Ltd.) with the production resistivity > 10 MΩ-
482 cm and TOC concentration < 5 ppb. The solute content in the water suspension was 0.06 wt%.
483 For mixed particles, the ratios of soluble components to silica were 1:19, 1:9 and 1:3, implying

484 that the fractions of soluble species were expected to be 5%, 10% and 25% of total particulate
485 mass in the atomized solution. We use the term solution, despite the fact that the insoluble silica
486 particles were suspended in the water (instead of dissolved).

487 _____After the particles had been produced they were fed into a diffusion drier (Fig. 1)
488 consisting of a porous tube surrounded by silica gel (Rotronic AG, model HC2-C04), resulting
489 in a relative humidity (RH) below 5% and they were neutralized using a charge neutralizer.
490 Thereafter particle number size distributions were measured using a Scanning Mobility Particle
491 Sizer (SMPS). The SMPS system was composed of an electrostatic classifier, which included
492 a Differential Mobility Analyzer (DMA) (Model 3071; TSI, Inc.) to bin the particles according
493 to electrical mobility, and an ultrafine Condensation Particle Counter (CPC Model 3025; TSI,
494 Inc.) to count the size-binned particles exiting the DMA.

495 Simultaneously, size-resolved CCN activity of the generated particles was measured
496 using a CCN counter (CCNc; Droplet Measurement Technologies Inc.) (Roberts and Nenes,
497 2005) (Fig.1). Before entering the CCNc, particles were size classified by a DMA, of the same
498 model as the DMA used in the SMPS. The CCNc operates by supersaturating sample air to the
499 point where the CCN become detectable particles. Humidified sheath air ($454 \text{ cm}^3 \text{ min}^{-1}$)
500 surrounds the sample flow ($45.4 \text{ cm}^3 \text{ min}^{-1}$) in the CCN column to hold it in the centre of the
501 column in the region of maximum supersaturation. The ratio of the flows was around 1 part of
502 sample air to 10 parts of sheath air and the total flow rate was $500 \text{ cm}^3 \text{ min}^{-1}$. The
503 supersaturation in the column can ~~can~~ be varied between 0.1% and 1.5%. The total number
504 concentration of the particles entering the CCNc was measured by a CPC (Model 3772; TSI,
505 Inc.) and the number of activated droplets was counted by an Optical Particle Counter (OPC)
506 over 20 size bins in the diameter range from 0.75 to 10 μm .

507 The effect of the silica particle morphology on activation was investigated by measuring
508 the mass of size classified particles by Aerosol Particle Mass Analyzer (APM) (model APM-
509 3600; Kanomax Inc.) (Fig. 1) (McMurry et al., 2002; Park et al., 2003a and 2003b). The APM
510 provides a direct relationship between the applied voltage, rotation speed, and particle mass
511 (Liu et al., 2012). Therefore, by measuring the outlet number concentration of the APM
512 corresponding to different applied voltages of the instrument, it was possible to measure the
513 mass distribution of the size selected particles. For each APM voltage, the downstream number
514 concentration was measured by a CPC (Model 3772; TSI, Inc.) (Fig. 1). From the voltage
515 corresponding to the highest concentration the average particle mass was calculated using the
516 following equation (McMurry et al., 2002; Park et al., 2003b):

$$m = \frac{qV}{r^2 \omega^2 \ln(r_2/r_1)} \quad (1)$$

where m is the particle mass, ω is the APM angular speed, V is the applied voltage, q is the particle charge, and r_1 , r_2 and r are the inner, outer and rotating radius of the instrument, respectively.

3 Theoretical frameworks

3.1 Non-sphericity of particles

Particle shape can affect the physical dimensions of the particle in terms of the surface available for water vapour to adsorb onto, as well as for the effective curvature determining the Kelvin effect (see e.g. Kumar et al., 2011a). In the case of highly non-spherical or porous particles the conversion between the electrical mobility (the quantity measured with the SMPS system) and the available surface area or particle volume and density is not straight-forward. As mentioned above, we used measurements of particle mass for the pure silica agglomerates to complement the information about the mobility of these particles.

Two parameters, the dynamic shape factor (χ) and fractal dimension (D_f), have been widely used to characterize non-sphericity of aerosol particles. Dynamic shape factor is defined as the ratio of the drag force on the agglomerated particles to the drag force on the volume equivalent spherical particles (χ' , volume-based shape factor) or to the drag force on the mass equivalent spherical particles (χ , mass-based shape factor) (DeCarlo et al., 2004; Fuchs, 1964; Kelly and McMurry, 1992; Kumar et al., 2011b) (DeCarlo et al., 2004; Kelly and McMurry, 1992), and The fractal dimension (D_f) is the coordination number in the aggregate and links properties like surface area of a particle to the scale of the measurements (Hinds, 1999; Ibaseta and Biscans, 2010). These parameters are applicable to quantify the morphology of agglomerated particles.

The mass-based shape factor is defined as (Kelly and McMurry, 1992):

$$\chi = \chi = \frac{d_b}{d_{me}} \cdot \frac{C(d_{me})}{C(d_b)} \quad (2)$$

where d_b and d_{me} are mobility diameter and mass equivalent diameter, while $C(d_b)$ and $C(d_{me})$ are the corresponding Cunningham slip correction factors. The slip correction factors are given by (Kulkarni, et al., 2011):

$$C(d_i) = 1 + \frac{2\lambda}{d_i} \left(1.142 + 0.558 \exp\left(-0.999 \frac{d_i}{2\lambda}\right) \right) \quad (3)$$

where λ is the mean free path of the gas molecules and d_i corresponds to either of d_{me} or d_b .
 The mass equivalent diameter (d_{me}) was calculated using the following equation (Kelly and McMurry, 1992):

$$d_{me} = \left(\frac{6m}{\pi\rho_p} \right)^{1/3} \quad (4)$$

where ρ_p is the material density of the silica particle (see Table 1)

To calculate the volume and surface equivalent diameters (d_{ve} and d_{se}) of the silica particles, which will be required to estimate the CCN capability of these particles, in addition to the mobility and mass data, knowledge on the volume-based shape factor (χ') is also required (see DeCarlo et al., 2004 and Kumar et al. 2011a for details):

$$\frac{d_{ve}}{C(d_{ve})} = \frac{d_b}{\chi \cdot C(d_b)} \quad (5)$$

$$d_{se} = \frac{3\chi d_{ve} - d_b}{2} \quad (6)$$

In this regard two limiting assumptions can be made. The first one is to assume compact agglomerates with nearly spherical shape and internal voids. In this case the mobility and volume equivalent diameters are approximately equal ($\chi' \approx 1$) and also equal to the surface equivalent diameter, but larger than the mass equivalent diameter, i.e. $d_b \approx d_{ve} \approx d_{se} > d_{me}$. The particle density is in this case lower than the pure silica material density, but equal to the effective density. The second assumption is to approximate the silica particles as chain-like agglomerates with no internal voids, for which mass and volume equivalent diameters are equal ($\chi \approx \chi'$), but smaller than surface equivalent and mobility diameters, i.e. $d_{ve} \approx d_{me} \leq d_{se}$ and d_b . In this case the particle density would be the same as the pure silica material density but higher than the effective density.

The fractal dimension (D_f) of the silica particles provides further insight on their sphericity (Boldridge, 2010; DeCarlo et al., 2004; Keskinen et al., 2011): for perfect spheres $D_f = 3$ and for line-like structures $D_f = 1$.

The fractal dimension of the pure silica particles was determined using the scaling law for effective density versus mobility diameter (Skillas et al., 1998, 1999):

$$\rho_e \propto d_b^{(D_f-3)} \quad (7)$$

is particle bulk density and where ρ_e is the particle effective density. The effective density of particles (ρ_e) was estimated using the following equation (Virtanen et al., 2004)(Kelly and McMurry, 1992; Park et al., 2003a; Virtanen et al., 2004; Liu et al., 2012):

577 $\rho_e = m/(\pi d_b^3/6);$ (38)

578 where m is the mass of the particles determined by using APM (Eq. 1). The mass equivalent
 579 diameter (\bar{d}_m) was calculated by the following equation (Kelly and McMurry, 1992):

580
$$\bar{d}_m = \left(\frac{m}{\rho_p} \right)^{1/3} \quad (4)$$

581 where ρ_p is the material density of the silica particle (see Table 1)

582 Slip correction factors are given by (Kulkarni, et al., 2011; Kumar et al., 2011b):

583
$$C = 1 + \frac{6\lambda}{d_p} \quad (5)$$

584 where λ is the mean free path of the gas molecules and corresponds to either of or:

585 The fractal dimension of the particles was determined using the scaling law for effective density
 586 versus mobility diameter (Skillas et al., 1998, 1999; Virtanen et al., 2004):

587
$$\rho_e \propto d_m^{-D} \quad (6)$$

588 After estimating the shape factor of the aggregates, the volume equivalent diameter (\bar{d}_v) and
 589 surface equivalent diameter of the particles were calculated using the following relations
 590 (DeCarlo et al., 2004; Kumar et al., 2011a):

591
$$\bar{d}_v = \left(\frac{m}{\rho_p} \right)^{1/3} \quad (7)$$

592
$$\bar{d}_s = \left(\frac{m}{\rho_p} \right)^{1/3} \quad (8)$$

593 The effect of non-sphericity on CCN activation was accounted for by using the surface
 594 equivalent diameter (\bar{d}_s), instead of mobility diameter (d_m), for pure and mixed silica particles. From
 595 here on we will thus use to denote the surface equivalent diameter.

596

597 3.2 CCN activation of soluble particles

598 κ -Köhler theory (Petters and Kreidenweis, 2007) was used to estimate the critical
 599 supersaturation of pure ammonium sulphate, sucrose and BSA particles. The saturation ratio
 600 (S) is expressed as:

601
$$S = \frac{d_p^3 - d_{dry}^3}{d_p^3 - d_{dry}^3(1-\kappa)} \exp\left(\frac{4\sigma_w M_w}{RT\rho_w d_p}\right) \quad (9)$$

602 where σ_w is the water surface tension, ρ_w is the water density, M_w is the molar mass of water, R
 603 is the universal gas constant, T is the temperature, d_{dry} is the dry particle diameter, d_p is the
 604 droplet diameter and κ is the hygroscopicity parameter of soluble particles.

605 _____ The supersaturation (s) is equal to $(S-1)$ and is expressed as a percentage. The maximum
 606 value of the supersaturation is called critical supersaturation (s_c) – similar definition naturally
 607 holding for critical saturation ratio S_c as well. Thus, at the critical point:

$$608 \left. \frac{ds}{dd_p} \right|_{d_p=d_c} = 0 \quad (10)$$

609 where d_c is called the critical diameter. The κ values for pure soluble particles were extracted
 610 from previous studies or, in the case of BSA, derived by applying the following relation
 611 introduced by Petters and Kreidenweis (2007) to our observations of the critical
 612 supersaturations of the pure soluble particles:

$$613 \kappa = \frac{4A^3}{27d_{dry} \ln^2 S_c} \quad (11)$$

614 where S_c is the saturation ratio at the critical point, $A = \frac{4\sigma M_w}{RT\rho_w}$, $\sigma = 0.072 \text{ J/m}^2$, $T = 298.15 \text{ K}$, M_w
 615 $= 0.018 \text{ kg/mol}$ and $\rho_w = 1000 \text{ kg/m}^3$.

616 The pure soluble particles were assumed to be compact and spherical, and thus the
 617 mobility diameter was used as the d_{dry} in Eqs. 9-11.

618

619 3.3 CCN activation of insoluble silica

620 The critical supersaturation of pure silica particles was calculated using FHH adsorption theory
 621 (Sorjamaa and Laaksonen, 2007, Kumar et al., 2009 and Kumar et al., 2011a). In this case the
 622 relationship between water supersaturation s and particle size can be expressed as:

$$623 s = \frac{4\sigma_w M_w}{RT\rho_w d_p} - A_{FHH} \left(\frac{d_p - d_{dry}}{2d_{H_2O}} \right)^{-B_{FHH}} \quad (12)$$

624 where d_{H_2O} ($= 2.75 \text{ \AA}$) is the diameter of the water molecule, and A_{FHH} and B_{FHH} are the FHH
 625 adsorption isotherm parameters. The first and second terms on the right hand side of Eq. 12
 626 correspond to the contributions from the Kelvin and adsorption effects, respectively.

627 In the literature, different values of the parameters A_{FHH} and B_{FHH} for silica particles have
 628 been reported. Kumar et al. (2011a) obtained the values 2.95 and 1.36 for A_{FHH} and B_{FHH} of
 629 quartz silica, respectively, and Keskinen et al. (2011) assigned values of 4.82 and 2.16 for A
 630 and B for non-agglomerated fumed silica particles (Degussa, Aerosil-300) with the diameter of
 631 8 and 10 nm.

632 To yield a reasonable estimate of the surface available for adsorption, the surface
 633 equivalent diameter of the pure silica particles was used as d_{dry} in Eq. 12.

635 3.4 CCN activation of mixed soluble and insoluble particles

636 Kumar et al. (2011b) used adsorption activation theory assuming that the particles are spheres
 637 and presented a ~~shell and core~~ model describing mixed particles with an insoluble and a soluble
 638 fraction, the core consisting of insoluble dust, and the shell consisting of a layer of soluble salt.
 639 They ~~presumed that the soluble part coats the insoluble part and~~ introduced the following
 640 relation between water supersaturation, particle size and composition:

$$641 \quad S = \frac{4\sigma_w M_w}{RT\rho_w d_p} - \frac{\varepsilon_s d_{dry}^3 \kappa}{(d_p^3 - \varepsilon_i d_{dry}^3)} - A_{FHH} \left(\frac{d_p - \varepsilon_i^{1/3} d_{dry}}{2d_{H_2O}} \right)^{-B_{FHH}} \quad (13)$$

642 where ε_i and $\varepsilon_s = 1 - \varepsilon_i$ are the insoluble and soluble volume fractions in the dry particles and κ
 643 is the hygroscopicity parameter of the soluble part. A_{FHH} and B_{FHH} are the FHH adsorption
 644 isotherm parameters of the insoluble part, which is assumed to interact with the water through
 645 adsorption onto its surface.

646 To estimate the average insoluble volume fractions of the mixed particles, the following
 647 relation was used:

$$648 \quad \varepsilon_i = \frac{m_i / \rho_i}{m_i / \rho_i + m_s / \rho_s} \quad (14)$$

649 where m_i and m_s are the insoluble and soluble mass fractions in the total mixed aerosol
 650 population, and ρ_i and ρ_s are the densities of the insoluble and soluble parts, respectively. The
 651 bulk densities of the used components are listed in Table 1.

652 In the second term of Eq. 13 the volume equivalent diameter was used as d_{dry} , while the
 653 surface equivalent diameter was assumed to represent the d_{dry} in the last term.

655 4 Results and discussion

656 4.1 Particle size distributions

657 The SMPS measurements yielded the average number size distributions for silica particles
 658 mixed with $(NH_4)_2SO_4$, sucrose and BSA (Fig. 2). Figure 2a displays average number size
 659 distributions for particles made of pure fumed silica, pure $(NH_4)_2SO_4$ and particles made of

660 silica and different amounts of $(\text{NH}_4)_2\text{SO}_4$. As is evident in the figure, size distributions of
661 particles generated from pure silica or pure $(\text{NH}_4)_2\text{SO}_4$ are unimodal while size distributions of
662 particles generated from the silica- $(\text{NH}_4)_2\text{SO}_4$ mixtures are bimodal. The mean mobility
663 diameter is ~ 30 nm for the pure $(\text{NH}_4)_2\text{SO}_4$ particles, and approximately 150 nm for the pure
664 silica particles. The first mode of the bimodal size distributions, associated with particles
665 generated from the aqueous bulk mixtures, is centered at a diameter of less than 30 nm. The
666 second mode, with lower number concentration, is centered at approximately 150 nm. Fig. 2b
667 shows the average number size distributions of particles made of sucrose and silica. Particles
668 made of pure sucrose have a mean diameter of approximately 50 nm. Size distributions
669 associated with particles generated from the silica-sucrose mixtures are bimodal (Fig. 2b); the
670 first mode centered at a diameter of less than 50 nm and the second mode centered at a diameter
671 of about 150 nm. Similarly, Fig. 2c shows the average SMPS number size distributions of
672 particles made of silica and BSA. These data are comparable with previous two measurements
673 in Figs 2a-b. The particles made of the large BSA protein have a mean diameter of about 75
674 nm. The mode associated with particles made of a mixture of BSA and silica is centered at
675 about 150 nm.

676 In the case of mixed aerosols, the particles in the first mode of the bimodal size
677 distributions are likely pure soluble particles, while the second mode of the bimodal distribution
678 curves represents silica particles mixed with soluble species. Hence, when analysing the
679 activation behaviour of mixed particles we omitted the CCNc data of the smallest particles by
680 subtracting their contribution from the CCN numbers and restricted our analysis to particle sizes
681 larger than 100 nm.

682 ~~In order to~~ To estimate the average soluble volume (mass) fractions in the mixed particles,
683 we calculated the ~~amount fraction~~ amount fraction of soluble material ~~lost to~~ the first ~~pure~~ mode of the particle
684 size distributions and subtracted it from the total soluble mass. In this regard, we fitted log-
685 normal distribution curves to the number size distributions associated with particles from the
686 mixtures and estimated the volume and mass distributions related to each particle number size
687 distribution. Hereupon, it was possible to estimate the fraction of total soluble mass remaining
688 in the first mode of the bimodal size distributions for each mixture, and the fraction of ~~the~~ total
689 soluble mass which was mixed with silica (Table 2). By multiplying this fraction with the
690 soluble mass fraction in the bulk mixture we gained an estimate of the real average soluble mass
691 fraction in the mixed/coated particles excluding the portion of the pure soluble particles. As is

692 evident from Table 2, the overall mass losses of the soluble materials from the first mode are
693 small, and 87-100% of the total soluble masses were mixed with silica particles.

695 **4.2 Mass analysis and size characterization of pure and mixed silica particles**

696 Since fumed silica particles are agglomerates, mass analysis of the pure silica particles could
697 help us to get a better understanding of their shape (see Sect. 3.1). ~~Therefore, we estimated the~~
698 ~~effective density and shape factor for these particles.~~ As an example, Figure 3a shows the
699 observed average number concentrations of 100 nm size-selected silica particles (by DMA) for
700 different APM voltages. A log-normal distribution was fitted to provide the voltage value
701 corresponding to the peak of the distribution. After determining the mass of size selected
702 particles using Eq. 1, the effective density of the silica particles was estimated (Eq. 3). The
703 APM measurements were performed for two different rotation speeds of the APM (3000 and
704 5000 rpm). The achieved effective particle densities using these two rotation speeds are
705 presented in Fig. 3b. There is only a small difference in effective density between the two
706 different speeds, giving confidence in the results. Figure 3c displays the mass-based shape
707 factor (χ) of silica particles for different mobility diameters. χ is clearly larger than 1 and
708 increases by increasing mobility diameter. This indicates that internal voids and/or irregularities
709 of the particles increase with increasing particle diameter (Kelly and McMurry, 1992).

710 ~~Afterward, the~~ The fractal dimension of the silica particles was estimated using the slopes
711 of the curves in Fig. 3b and Eq. 6 ~~yielding D_f The slope values, of 2.54 and 2.55, for the were~~
712 ~~fitted respectively for of the silica particles in 3000 and 5000 rpm rotation speeds, thus~~
713 ~~suggesting closer to spherical rather than rod- or chain-like structures. of the APM instrument.~~
714 Fitted The fitted D_f values are also close to the value ($D_f=2.57$) reported by Keskinen et al.
715 (2011) and Ibaseta and Biscans (2010) ($D_f=2$ to 2.5) for fumed silica (Degussa, Aerosil-300
716 and -200, respectively). We therefore expect the silica particles to be better represented by the
717 “compact agglomerates” assumption and applying this assumption ($\chi'=1$, see Sect. 3.1), the
718 volume and surface equivalent diameters used in all the CCN activity calculations were thus
719 approximated with the mobility diameters. Figure 3c displays the dynamic shape factor of silica
720 particles for different mobility diameters. The shape factor of the silica particles increases by
721 increasing mobility diameter, which indicates that irregularities in particle shape or internal
722 voids within the particles increase with increasing particle diameter (Kelly and McMurry,
723 1992). By using the derived shape factors the surface equivalent diameter corresponding to

724 ~~different mobility diameters of silica particles (using Eq. 8) could be estimated (Fig. 3d). As~~
725 ~~expected, because of the void spaces inside the silica agglomerates, the surface equivalent~~
726 ~~diameter for silica particles is larger than its corresponding mobility diameter. The surface~~
727 ~~equivalent diameter was then used in all the theoretical calculations to represent the physical~~
728 ~~size of the particles in Eqs. 12–13.~~

729 The mass analysis results were only available for the pure silica particles. When analysing
730 the CCN activation data for the mixed particles, we assumed that the effective density of the
731 silica in the mixed particles was similar to the effective density of the pure silica particles. The
732 physical meaning of this assumption would be that the silica present in the mixed particles
733 would contain the same volume of voids per unit silica mass as the pure particles. Furthermore,
734 when calculating the critical supersaturations using Eq. 13 the adsorption term was calculated
735 using the surface equivalent diameter d_{se} as d_{dry} and the solubility term using the volume
736 equivalent diameter d_{ve} as d_{dry} , which in our case, by compact agglomerates assumption d_{ve}
737 $\equiv d_{se} \equiv d_b$.

739 **4.3 CCN activation results**

740 Before analysing the CCN activity of the generated particles, all the activation curves were
741 charge-corrected using the procedure introduced by Moore et al. (2010). The ratio of the
742 corrected CCN and CN (Condensation Nuclei, measured by CPC) time series thus determines
743 the activated fraction (also referred to as activation ratio) of the specified particles (Kumar et
744 al., 2011a). Furthermore, as described in Sec. 4.3.2, for the mixed particles the contributions of
745 the smaller completely soluble particle mode (see Fig. 2) were subtracted from the CCN
746 concentrations. Finally all the activation curves used in the further analysis were normalized
747 using a correction factor derived from the ammonium sulphate (AS) experiments, assuming that
748 AS activation probability reaches unity at high supersaturations. In the cases where the
749 normalization with the AS data would have produced CCN/CN values larger than unity, the
750 value was set to unity instead.

752 **4.3.1 CCN behavior of pure components**

753 Figure 4 shows the activation ratio dependence on supersaturation for 120 nm (mobility
754 diameter) pure silica, BSA, sucrose and ammonium sulphate particles. A sigmoid curve was
755 fitted to each set of activation ratio data. Critical supersaturation (s_c) is often associated with

756 the supersaturation where 50% of the particles are CCN activated – equivalent to a CCN/CN-
757 ratio of 50%, and we will follow this convention although the two are not necessarily equal
758 when the CCN/CN curve is not a step function. As expected, $(\text{NH}_4)_2\text{SO}_4$ particles, which are
759 the most hygroscopic particles investigated in this study (see κ values in Table 1), activated at
760 lower supersaturations than was the case for sucrose, silica and BSA particles. The pure silica
761 particles, which are insoluble and non-hygroscopic, exhibited the highest critical
762 supersaturation of the investigated compounds (Fig. 4).

763 Figure 5 displays activation ratio against supersaturation for pure silica particles of
764 different mobility diameters. As is evident from Fig. 5, the critical supersaturation decreases
765 with increasing particle diameter. Experimentally and theoretically determined critical
766 supersaturations of pure silica particles as a function of particle mobility diameter are shown in
767 Fig. 6. Previously, the values for FHH adsorption parameters (Eqs. 10 and 12) of different
768 types of silica have been determined by Kumar et al. (2011a) (quartz), and Keskinen et al.
769 (2011) (Fumed silica, Aerosil-300). To compare our results (~~Fumed silica, Aerosil-90~~) of the
770 ~~pure silica activation~~ to these studies, we fitted the FHH adsorption parameters for the pure
771 silica particles (Fumed silica, Aerosil-90). A_{FHH} and B_{FHH} values of 2.50 and 1.9-62 explain our
772 results on the activation diameter vs. critical supersaturation (Fig. 6), although the fits were
773 difficult to constrain uniquely. ~~The results indicate, however, that o~~Our results are closer to
774 those reported by ~~better in line with the work of~~ Keskinen et al. (2011) than Kumar et al. (2011a)
775 ~~, but although~~ the A_{FHH} and B_{FHH} values are close to those reported by Kumar et al. (2011a).
776 This highlights the sensitivity of the fits to ~~these values~~adsorption parameters, reflecting the
777 fact that our data set is not sufficient for constraining any physical or chemical phenomena
778 behind these values. In particular, the parameter A_{FHH} , describing the interactions of the first
779 monolayer with the adsorbent surface, seems to be difficult to constrain based on the CCN
780 activation data. This is perhaps not surprising as at the point of activation the rapid condensation
781 of water might relatively soon destroy the information of the very first steps of the adsorption /
782 monolayer formation. For the parameter B_{FHH} , on the other hand, the fits seem to reproduce
783 relatively robust values. CCN activation measurements are probably not the best approach for
784 yielding accurate data of the physical phenomena behind the adsorption parameters – as a lot
785 of information has already been lost at the point where the CCN are activated and detected –
786 but should be rather regarded as a valuable source of information on the processes limiting
787 atmospheric cloud droplet formation. It ~~must~~should also be pointed out that the quartz silica
788 (Kumar et al., ~~2009~~2011a) is not as hydrophilic as fumed silica which probably affects the

789 critical supersaturation. Furthermore, the FHH adsorption parameters in Keskinen et al. (2011)
790 study were fitted for only 8 and 10 nm fumed silica particles which were most likely spherical
791 and thus potentially not fully representative of the agglomerated particles that we used. Impurity
792 of the silica could also affect the results even though the deionized water conditions were as
793 pure as possible was used in all studies. To conclude, the experimental results for s_c of pure
794 silica particles were in good agreement with theoretical calculations using FHH adsorption
795 isotherm and small deviations were only observed for larger diameters.

796 To estimate the critical supersaturations of pure soluble particles, κ -Köhler theory (Eqs.
797 9 and 10) was applied. Table 1 lists κ values of the soluble materials used in this study. The
798 ability for ammonium sulphate particles to act as CCN has been widely studied (e.g. Garland,
799 1969; Kreidenweis et al., 2005; Hiranuma et al., 2011), and here we employed the previously-
800 reported hygroscopicity (κ) values (Petters and Kreidenweis, 2007), given the relatively good
801 agreement between the κ value fitted to our results (0.78) and the literature values. The κ value
802 for pure sucrose was extracted from Ruehl et al. (2010), which was also in reasonable agreement
803 with the value 0.08 that best described our results. For the pure BSA particles κ was calculated
804 based on Eq. 11 using the CCN activation results of pure BSA particles in this study. The
805 experimentally and theoretically determined critical supersaturations for pure $(\text{NH}_4)_2\text{SO}_4$, BSA
806 and sucrose particles are shown in Fig. 7. Indeed, κ -Köhler theory results using the literature
807 values for the hygroscopicity parameter were in good agreement with the experimentally
808 determined critical supersaturations of pure soluble particles.

809

810 4.3.2 CCN behavior of the mixtures

811 Here we present the CCN activation results of co-synthesized silica particles mixed with
812 $(\text{NH}_4)_2\text{SO}_4$, sucrose or BSA considering the determined total soluble fractions in the mixed
813 particle population from Table 2.

814 The activation ratio curves were determined for different diameters of mixed particles
815 and different ratios of soluble to insoluble materials. For mixed particles the activation ratio
816 curves were modified by subtracting the contributions of the smaller completely soluble particle
817 from the CCN and CN concentrations using the following procedure: First, the contribution of
818 pure soluble particles to the total number of CN for each size were estimated by fitting two log-
819 normal modes to the size distributions such as those shown in Fig. 2. The pure soluble mode
820 was then subtracted from the CN data for each size to yield an estimate of the total numbers of

821 mixed CN. Second, using the CCN/CN ratios of the pure soluble particles (shown for 120 nm
822 in Fig. 4) we could estimate the number of CCN originating from pure CN at each mobility
823 diameter and supersaturation. Subtracting this from the total number of CCN, we could yield
824 an estimate for the CCN/CN ratio for the mixed particles. Figure 8 ~~shows~~ represents the
825 activation ratio curves for 150 nm (mobility diameter) pure and mixed particles. Although both
826 the raw data (unnormalized) and the normalized curves are shown for completeness, only the
827 normalized data was used in the follow-up analysis. It can be seen that the normalization
828 procedure caused only very small adjustments to the 50% points inferred from the curves.

829 _____ Figure 8a shows the activation probabilities of mixed silica-(NH₄)₂SO₄ particles. The
830 critical supersaturation (corresponding to CCN/CN=50%) is higher for pure silica particles than
831 for the particles with soluble material. Evidently, the pure (NH₄)₂SO₄ particles have the lowest
832 critical supersaturation. Furthermore, the critical supersaturation decreases when the fraction of
833 soluble material in the particles increases, and the CCN/CN curves are shallower (i.e. further
834 from a step function) for the mixed as compared with the pure particles. The same behavior can
835 be observed in Fig. 8b for 150 nm silica particles mixed with sucrose. Pure sucrose particles
836 were activated at a supersaturation of 0.22% which is comparable to previous studies of sucrose
837 (e.g. Rosenorn et al., 2006). s_c decreases with increasing sucrose ratio in the mixed particles,
838 similar to what was observed for ammonium sulphate in Fig. 8a. In the case of particles
839 containing BSA, however, a different behavior was observed: s_c was higher for particles made
840 of 5% and 10% BSA than for particles made of pure silica (Fig. 8c). The reason for this behavior
841 is not clear but it is known that adsorption of BSA on silica can affect the structural properties
842 of BSA. As was explained by Larsericsdotter et al. (2005), for soft proteins such as BSA the
843 structural stability decreases when adsorption onto other materials occurs. On the other hand,
844 the BSA can also affect the agglomerate structure of the mixed particles – for instance through
845 more compact agglomerates with increasing BSA concentrations (see e.g. Kiselev et al., 2010
846 and Stratmann et al., 2010 for discussion on effects of coating on agglomerate compactness).
847 However, it is also possible that this effect is solely due to different distribution of the soluble
848 materials as a function of particle size for the different bulk solution compositions, which is
849 discussed in detail below.

850 To estimate the soluble mass fractions (ω_s) in the coated/mixed particles required for the
851 application of Eq. 13, the total amount of soluble coating-material was first estimated by fitting
852 log-normal size distributions to the observed size distributions (Sect. 4.1). The dashed lines in
853 Fig. 9 show the theoretical critical supersaturations (using Eq. 13) of particles consisting of a

854 mixture of silica and ammonium sulphate assuming soluble volume fractions (ε_s)
855 corresponding to these constant ω_s (see Table 2 and the dashed lines of the insert in
856 Fig. 9) with changing diameter. These theoretical values of critical supersaturations are mostly
857 lower than the observed critical supersaturations (stars), and the size-dependence of the critical
858 supersaturation is not captured by the theory. We observed the same (although less pronounced)
859 behavior for silica particles mixed with sucrose and BSA (Figs. 10 and 11). In all three cases,
860 the observed critical supersaturations were higher than expected from the ~~shell-core~~ model by
861 Kumar et al. (2011b) using constant soluble mass fractions. The calculations are very sensitive
862 to the κ values and the deviation between experimental and estimated s_c for mixed particles
863 increases with increasing hygroscopicity. The largest deviations were observed for particles
864 mixed with $(\text{NH}_4)_2\text{SO}_4$, which is more hygroscopic ($\kappa=0.61$) than the other compounds, and the
865 smallest deviations were observed for silica particles mixed with BSA which has the lowest
866 hygroscopicity ($\kappa=0.01$). The adsorption term contribution to the critical supersaturation in Eq.
867 13 was generally minor: <0.72% for silica + $(\text{NH}_4)_2\text{SO}_4$, <3.8% for silica + sucrose and <7%
868 for silica + BSA of the total (~~kelvin-Kelvin~~ + solubility + adsorption) contribution for all the
869 studied compositions and supersaturations. The theoretical predictions were thus dominated by
870 the Kelvin and solubility effects – similarly to the case of soot agglomerates studied by Henning
871 et al (2010).

872 The small contribution of the adsorption term to the theoretical predictions combined with
873 the shallow activation ratio curves (see Fig. 8) suggest that the reason for the apparent
874 discrepancy between the theoretical and the observed critical supersaturations is a non-constant
875 distribution of the soluble material with varying particle size. This explanation seems
876 particularly feasible taking into account the good agreement between the experiments and
877 theory for the pure particles, and the fact that the particle generation method (atomization and
878 drying of aqueous solutions) does not allow for controlling the ratio of soluble to insoluble
879 materials at a given particle size – only for the overall aerosol population. To yield further
880 insight into this, we estimated the distribution of the soluble material by fitting size-dependent
881 ε_s distributions to the CCN/CN vs. s_c curves (e.g. Fig. 8) using Eq. 13 – thus assuming that all
882 the mixed particles that activate at a given supersaturation interval contain a specific soluble
883 volume (mass) fraction. It is worthwhile to note that the ε_s determined this way correspond to
884 the surface or volume equivalent diameters (linked to the ~~particle mass-volume equivalent~~
885 ~~diameter~~ through the modified silica-effective density including internal voids, see Sect. 3), and
886 is thus not directly comparable to the mass fractions in the atomized solution.

887 The s_c (defined as the 50% point in the CCN/CN curves) vs. mobility diameter results
888 obtained through the fitting procedure are shown by the solid lines in Figs. 9-11, and the
889 resulting soluble mass fractions ω_s s corresponding to the ε_s s fitted to the 50% points in the
890 CCN/CN curves as a function of particle size are shown as the solid lines in the insets. The
891 results suggest a very uneven distribution of the soluble material as a function of particle size:
892 the small particles contain considerably higher fractions of soluble material than the larger ones,
893 and the effect increases with the amount of soluble material. In the case of BSA (Fig. 11), the
894 different mixture compositions lie relatively close to each other in terms of their critical
895 supersaturations – making it difficult to constrain the soluble contents of these particles.
896 However, it seems clear that at the small particle sizes (< 150 nm) the particle population is
897 dominated by pure BSA particles. At sizes between 150 and 250 nm, on the other hand,
898 extremely low BSA-content is required to reproduce the observed critical supersaturations. This
899 is of course also visible in Fig. 8c, where the mixtures with low BSA-content seem to activate
900 at even higher supersaturations than pure silica. The exact reason for this is not clear, but the
901 effect of BSA on silica particle structure (e.g. density etc.) could be speculated upon.
902 ~~, there even appears to be a large number of pure BSA particles present at the low end of the~~
903 ~~“mixed” size distribution governing the 50% activation point.~~

904 While the size-dependent ω_s shown in Figs. 9-11 correspond to the points at which 50%
905 of the CN activate as CCN for a given particle diameter and supersaturation, the ω_s values vary
906 even for a given particle size – as indicated by non-step function shape of the activation curves
907 in Fig. 8. An example distribution of the soluble mass as deduced from the CCN/CN vs. s_c data
908 (Fig. 8) using Eq. 13 is shown in Fig. 12 for the 150 nm mobility diameter mixed particles. The
909 figure shows that for each mixture, there is an uneven distribution of soluble mass fraction in
910 the particles of a given size ~~(here 150 nm)~~. In all cases, there ~~are~~ is a large ~~amount~~ number of
911 particles with very low soluble mass fractions (less than initial bulk solution) and the
912 composition of the size-selected particles is not constant. Similar conclusions were drawn by
913 Dusek et al. (2006) for soot particles coated by NaCl. When compared to the mass fractions in
914 the atomized solution, it can be seen that only in the case of sucrose the distribution peaks at
915 soluble mass fractions similar to the original solution, while the mixtures containing ammonium
916 sulphate and BSA have widely varying compositions.

917

918

919 **5 Summary and conclusions**

920 In this study, the CCN activation of pure and mixed particles of silica and soluble compounds
921 (AS, sucrose and BSA) was investigated. Furthermore, the morphology and effective density
922 of silica particles were investigated based on APM measurements. In addition, size distributions
923 of the sampled particles were measured using a SMPS. Then non-sphericity of the particles was
924 investigated by applying APM measurements and estimating mass-based dynamic shape factors
925 and fractal dimensions of pure silica particles. Assuming that our pure and mixed silica particles
926 are compact agglomerates, which is the most reasonable assumption for our silica particles with
927 fractal dimension of 2.54-2.55 close to the spherical particles with fractal dimension of three,
928 By using these derived shape factors, the surface and volume equivalent diameters
929 corresponding to different become identical to the mobility diameters of the silica-ese particles,
930 which was needed for the theoretical calculations, was estimated. The SMPS results showed
931 that the particles generated from pure compounds resulted in unimodal size distributions, while
932 the particles generated from mixtures were associated with bimodal size distributions. The first
933 peak of the bimodal size distribution indicated that also the mixture generated some pure soluble
934 particles. The size distributions allowed us to estimate the total soluble vs. insoluble mass
935 fractions present in the mixed particle population.

936 CCN activity measurements were conducted in various supersaturations up to 1.5%, and
937 activation ratio curves were determined for the evaluated particles. Afterward, the experimental
938 data were compared to theoretical values using adsorption theory (e.g. Sorjamaa and
939 Laaksonen, 2007) for the pure silica particles, κ -Köhler-theory (Petters and Kreidenweis, 2007)
940 for the pure soluble particles, and a shell and core model describing mixtures of soluble and
941 insoluble components introduced by Kumar et al. (2011b) for the mixed particles. The CCN
942 activation of pure soluble and insoluble particles was in good agreement with κ -Köhler theory
943 and adsorption theory. For mixed particles, however, the observed critical supersaturations
944 were higher than those expected from the shell and core model by Kumar et al. (2011b), if
945 constant soluble and insoluble mass fractions were assumed for the whole mixed particle
946 population. This indicates that the particles were less hygroscopic than expected, indicating an
947 uneven distribution of the soluble material in the aerosol size distribution. As the calculations
948 were governed by the soluble mass (volume) fraction in the particles instead of adsorption
949 effects, we could use the experimental critical supersaturations to estimate size-dependent
950 distribution of the soluble material in the mixed particles. For particles > 150 nm in mobility
951 diameter the soluble fractions were smaller and for particles < 150 nm mostly larger than in the

952 total mixed particle population – indicating that the soluble material preferentially accumulated
953 to particles < 150 nm, independent of the exact identity of the soluble species. If the uneven
954 distribution of the soluble material was accounted for, the framework by Kumar et al. (2011b)
955 could be successfully used to describe the CCN activation of insoluble particles mixed with
956 soluble pollutants.

957 Our results indicate that knowing the fraction of soluble material (instead of the
958 adsorption properties of the surfaces) is the key prerequisite for describing the CCN activation
959 of silica mixed with soluble pollutants – at least for the relatively large soluble fractions studied
960 here. ~~Our mixed particles consistent of varying soluble fractions, thus probably representing an~~
961 ~~aerosol population with various degrees of aging in the atmosphere.~~ Furthermore, our results
962 indicate that well-defined descriptions of the coating processes are crucial for elucidating the
963 phenomena governing the CCN activation of insoluble particles mixed with soluble
964 compounds. We also conclude that although the model by Kumar et al. (2011b) was originally
965 introduced for fresh dust coated by a layer of soluble salt after ageing, it gives a reasonable
966 estimate of the potential importance of adsorption as compared with the bulk solubility of the
967 mixed soluble-insoluble particles.

968

969 *Acknowledgements*

970 Financial support from the Nordic Centre of Excellence CRAICC (Cryosphere-atmosphere
971 interactions in a changing Arctic climate), Vetenskapsrådet (grant n:o 2011-5120), Academy of
972 Finland (272041, 259005, [283031](#) and [138951](#)) and the European Research Council (StG n:o
973 27877 ATMOGAIN and 335478 QAPPA) is gratefully acknowledged.

974

975 **References**

- 976 Biskos, G., Russell, L. M., Buseck, P. R. and Martin, S. T.: Nanosize effect on the hygroscopic
977 growth factor of aerosol particles, *Geophys. Res. Lett.*, 33(7), L07801,
978 doi:10.1029/2005GL025199, 2006.
- 979 Boldridge, D.: Morphological characterization of fumed silica aggregates, *Aerosol Sci.*
980 *Technol.*, 44(3), 182–186, doi:10.1080/02786820903499462, 2010.
- 981 DeCarlo, P. F., Slowik, J. G., Worsnop, D. R., Davidovits, P. and Jimenez, J. L.: Particle
982 morphology and density characterization by combined mobility and aerodynamic diameter
983 measurements. Part 1: theory, *Aerosol Sci. Technol.*, 38(12), 1185–1205,
984 doi:10.1080/027868290903907, 2004.
- 985 Dusek, U., Reischl, G. P. and Hitzenberger, R.: CCN activation of pure and coated carbon black
986 particles, *Environ. Sci. Technol.*, 40, 1223–1230, 2006.
- 987 Fuchs, N. A.: *The mechanics of aerosols*, Pergamon Press, London., 1964.
- 988 Garland, J. A.: Condensation on ammonium sulphate particles and its effect on visibility, *Atmos.*
989 *Environ.*, 3, 347–354, 1969.
- 990 Grayson, M., Ed.: *Encyclopedia of glass, ceramics and cement*, John Wiley & Sons, Inc, New
991 York., 1985.
- 992 Haynes, W. M., Bruno, T. J. and Lide, D. R., Eds.: *CRC handbook of chemistry and physics*,
993 94th ed., CRC Press. [online] Available from: <http://www.hbcnpnetbase.com/>, last access: 19
994 July 2013, 2013.
- 995 Haywood, J. and Boucher, O.: Estimates of the direct and indirect radiative forcing due to
996 tropospheric aerosols: A review, *Rev. Geophys.*, 38(4), 513–543, 2000.
- 997 Henning, S., Wex, H., Hennig, T., Kiselev, a., Snider, J. R., Rose, D., Dusek, U., Frank, G. P.,
998 Pöschl, U., Kristensson, a., Bilde, M., Tillmann, R., Kiendler-Scharr, a., Mentel, T. F., Walter,
999 S., Schneider, J., Wennrich, C. and Stratmann, F.: Soluble mass, hygroscopic growth, and
1000 droplet activation of coated soot particles during LACIS Experiment in November (LExNo), *J.*
1001 *Geophys. Res.*, 115(D11), D11206, doi:10.1029/2009JD012626, 2010.
- 1002 Hinds, W. C.: *Aerosol technology: properties, behavior, and measurement of airborne particles*,
1003 2nd ed., John Wiley & Sons Inc., New York., 1999.
- 1004 Hings, S. S., Wrobel, W. C., Cross, E. S., Worsnop, D. R., Davidovits, P. and Onasch, T. B.:
1005 CCN activation experiments with adipic acid: effect of particle phase and adipic acid coatings
1006 on soluble and insoluble particles, *Atmos. Chem. Phys.*, 8, 3735–3748, doi:10.5194/acp-8-
1007 3735-2008, 2008.
- 1008 Hiranuma, N., Kohn, M., Pekour, M. S., Nelson, D. a, Shilling, J. E. and Cziczo, D. J.: Droplet
1009 activation, separation, and compositional analysis: laboratory studies and atmospheric
1010 measurements, *Atmos. Meas. Tech.*, 4(10), 2333–2343, doi:10.5194/amt-4-2333-2011, 2011.

- 1011 Ibaseta, N. and Biscans, B.: Fractal dimension of fumed silica: Comparison of light scattering
1012 and electron microscope methods, *Powder Technol.*, 203(2), 206–210,
1013 doi:10.1016/j.powtec.2010.05.010, 2010.
- 1014 IPCC: (Intergovernmental Panel on Climate Change): *Climate Change 2013, The Physical*
1015 *Science Basis*, Cambridge University Press, Cambridge., 2013.
- 1016 Jacob, D. J.: *Introduction to atmospheric chemistry*, Princeton University Press, Princeton.
1017 [online] Available from: <http://www.ncbi.nlm.nih.gov/pubmed/14664619>, 1999.
- 1018 Jeyachandran, Y. L., Mielczarski, J. a, Mielczarski, E. and Rai, B.: Efficiency of blocking of
1019 non-specific interaction of different proteins by BSA adsorbed on hydrophobic and hydrophilic
1020 surfaces., *J. Colloid Interface Sci.*, 341(1), 136–42, doi:10.1016/j.jcis.2009.09.007, 2010.
- 1021 Kelly, W. P. and McMurry, P. H.: Measurement of particle density by inertial classification of
1022 Differential Mobility Analyzer-generated monodisperse aerosols, *Aerosol Sci. Technol.*, 17,
1023 199–212, 1992.
- 1024 Keskinen, H., Romakkaniemi, S., Jaatinen, A., Miettinen, P., Saukko, E., Jorma, J., Mäkelä, J.
1025 M., Virtanen, A., Smith, J. N. and Laaksonen, A.: On-line characterization of morphology and
1026 water adsorption on fumed silica nanoparticles, *Aerosol Sci. Technol.*, 45(12), 1441–1447,
1027 doi:10.1080/02786826.2011.597459, 2011.
- 1028 Kiselev, a., Wennrich, C., Stratmann, F., Wex, H., Henning, S., Mentel, T. F., Kiendler-Scharr,
1029 a., Schneider, J., Walter, S. and Lieberwirth, I.: Morphological characterization of soot aerosol
1030 particles during LACIS Experiment in November (LExNo), *J. Geophys. Res.*, 115(D11),
1031 D11204, doi:10.1029/2009JD012635, 2010.
- 1032 Kreidenweis, S. M., Koehler, K., DeMott, P. J., Prenni, a J., Carrico, C. and Ervens, B.: Water
1033 activity and activation diameters from hygroscopicity data - Part I: Theory and application to
1034 inorganic salts, *Atmos. Chem. Phys.*, 5(5), 1357–1370 [online] Available from:
1035 <http://www.atmos-chem-phys.net/5/1357/2005/>, 2005.
- 1036 Kulkarni, P.; Baron, P.A.; Willeke, K., Ed.: *Aerosol measurement: principles, techniques, and*
1037 *applications*, 3rd ed., John Wiley & Sons, Inc., Hoboken, New Jersey., 2011.
- 1038 Kumar, P., Sokolik, I. N. and Nenes, a.: Parameterization of cloud droplet formation for global
1039 and regional models: including adsorption activation from insoluble CCN, *Atmos. Chem.*
1040 *Phys.*, 9(7), 2517–2532, doi:10.5194/acp-9-2517-2009, 2009.
- 1041 Kumar, P., Sokolik, I. N. and Nenes, a.: Measurements of cloud condensation nuclei activity
1042 and droplet activation kinetics of fresh unprocessed regional dust samples and minerals, *Atmos.*
1043 *Chem. Phys.*, 11(7), 3527–3541, doi:10.5194/acp-11-3527-2011, 2011a.
- 1044 Kumar, P., Sokolik, I. N. and Nenes, a.: Cloud condensation nuclei activity and droplet
1045 activation kinetics of wet processed regional dust samples and minerals, *Atmos. Chem. Phys.*,
1046 11(16), 8661–8676, doi:10.5194/acp-11-8661-2011, 2011b.

- 1047 Larsericsdotter, H., Oscarsson, S. and Buijs, J.: Structure, stability, and orientation of BSA
1048 adsorbed to silica., *J. Colloid Interface Sci.*, 289(1), 26–35, doi:10.1016/j.jcis.2005.03.064,
1049 2005.
- 1050 Levin, E. L., Spector, P. E., Menon, S., Narayanan, L. and Cannon-Bowers, J. a: The effects of
1051 desert particles coated with sulfate on rain formation in the eastern Mediterranean, *Hum.*
1052 *Perform.*, 9(1), 1511–1523 [online] Available from:
1053 http://www.tandfonline.com/doi/abs/10.1207/s15327043hup0901_1, 1996.
- 1054 Liu, Q., Ma, X. and Zachariah, M. R.: Combined on-line differential mobility and particle mass
1055 analysis for determination of size resolved particle density and microstructure evolution,
1056 *Microporous Mesoporous Mater.*, 153, 210–216, doi:10.1016/j.micromeso.2011.11.017, 2012.
- 1057 Lohmann, U. and Feichter, J.: Global indirect aerosol effects: a review, *Atmos. Chem. Phys.*,
1058 5(3), 715–737 [online] Available from: <http://hal-insu.archives-ouvertes.fr/hal-00295633/>,
1059 2005.
- 1060 Mackay, J. and Mensah, G. A.: Atlas of heart disease and stroke, World Health Organization
1061 (WHO), Geneva,., 2004.
- 1062 McCormick, R. A. and Ludwig, J. H.: Climate modification by atmospheric aerosols, *Science*,
1063 156, 1358–1359, 1976.
- 1064 McMurry, P. H., Wang, X., Park, K. and Ehara, K.: The relationship between mass and mobility
1065 foratmospheric particles: a new technique for measuring particle density, *Aerosol Sci. Technol.*,
1066 36(2), 227–238, doi:10.1080/027868202753504083, 2002.
- 1067 Mikhailov, E., Vlasenko, S. and Niessner, R.: Interaction of aerosol particles composed of
1068 protein and salts with water vapor : hygroscopic growth and microstructural rearrangement,
1069 *Atmos. Chem. Phys.*, 4, 323–350, 2004.
- 1070 Moore, R. H., Nenes, A. and Medina, J.: Scanning Mobility CCN Analysis—A method for fast
1071 measurements of size-resolved CCN distributions and activation kinetics, *Aerosol Sci.*
1072 *Technol.*, 44(10), 861–871, doi:10.1080/02786826.2010.498715, 2010.
- 1073 Park, K., Cao, F., Kittelson, D. B. and McMurry, P. H.: Relationship between particle mass and
1074 mobility for diesel exhaust particles., *Environ. Sci. Technol.*, 37(3), 577–83 [online] Available
1075 from: <http://www.ncbi.nlm.nih.gov/pubmed/12630475>, 2003a.
- 1076 Park, K., Kittelson, D. B. and McMurry, P. H.: A closure study of aerosol mass concentration
1077 measurements: comparison of values obtained with filters and by direct measurements of mass
1078 distributions, *Atmos. Environ.*, 37(9-10), 1223–1230, doi:10.1016/S1352-2310(02)01016-6,
1079 2003b.
- 1080 Petters, M. D. and Kreidenweis, S. M.: A single parameter representation of hygroscopic
1081 growth and cloud condensation nucleus activity, *Atmos. Chem. Phys.*, 7(8), 1961–1971,
1082 doi:10.5194/acp-7-1961-2007, 2007.
- 1083 Pope, C. A. and Dockery, D. W.: Health effects of fine particulate air pollution : lines that
1084 connect, *J. Air Waste Manage. Assoc.*, 56, 709–742, 2006.

- 1085 Pope, C. A., Ezzati, M. and Dockery, D. W.: Fine-particulate air pollution and life expectancy
1086 in the United States, *N. Engl. J. Med.*, 360(4), 376–386, 2009.
- 1087 Ramanathan, V., Crutzen, P. J., Kiehl, J. T. and Rosenfeld, D.: Aerosols, climate, and the
1088 hydrological cycle., *Science*, 294, 2119–24, doi:10.1126/science.1064034, 2001.
- 1089 Ravishankara, A. D.: Heterogeneous and multiphase chemistry in the troposphere, *Science*,
1090 276, 1058–1065, 1997.
- 1091 Roberts, G. and Nenes, A.: A continuous-flow streamwise thermal-gradient CCN chamber for
1092 atmospheric measurements, *Aerosol Sci. Technol.*, 39(3), 206–221,
1093 doi:10.1080/027868290913988, 2005.
- 1094 Rosenorn, T., Kiss, G. and Bilde, M.: Cloud droplet activation of saccharides and levoglucosan
1095 particles, *Atmos. Environ.*, 40(10), 1794–1802, doi:10.1016/j.atmosenv.2005.11.024, 2006.
- 1096 Ruehl, C. R., Chuang, P. Y. and Nenes, A.: Aerosol hygroscopicity at high (99 to 100 %)
1097 relative humidities, *Atmos. Chem. Phys.*, 1329–1344, 2010.
- 1098 Saathoff, H., Naumann, K.-H., Schnaiter, M., Schöck, W., Möhler, O., Schurath, U.,
1099 Weingartner, E., Gysel, M. and Baltensperger, U.: Coating of soot and (NH₄)₂SO₄ particles by
1100 ozonolysis products of α -pinene, *J. Aerosol Sci.*, 34(10), 1297–1321, doi:10.1016/S0021-
1101 8502(03)00364-1, 2003.
- 1102 Scheckman, J. H., McMurry, P. H. and Pratsinis, S. E.: Rapid characterization of agglomerate
1103 aerosols by in situ mass-mobility measurements., *Langmuir*, 25(14), 8248–54,
1104 doi:10.1021/la900441e, 2009.
- 1105 Seinfeld, J. H. and Pandis, S. N.: *Atmospheric Chemistry and Physics: From Air Pollution to*
1106 *Climate Change*, 2nd ed., 2006.
- 1107 Shiraiwa, M., Ammann, M., Koop, T. and Pöschl, U.: Gas uptake and chemical aging of
1108 semisolid organic aerosol particles., *Proc. Natl. Acad. Sci. U. S. A.*, 108(27), 11003–8,
1109 doi:10.1073/pnas.1103045108, 2011.
- 1110 Skillas, G., Kunzel, S., Burtscher, H., Baltensperger, U. and Siegmann, K.: High fractal-like
1111 dimension of diesel soot agglomerates, *J. Aerosol Sci.*, 29(4), 411–419, 1998.
- 1112 Skillas, G., Burtscher, H., Siegmann, K. and Baltensperger, U.: Density and fractal-like
1113 dimension of particles from a laminar diffusion flame., *J. Colloid Interface Sci.*, 217(2), 269–
1114 274, doi:10.1006/jcis.1999.6370, 1999.
- 1115 Sorjamaa, R. and Laaksonen, A.: The effect of H₂O adsorption on cloud drop activation of
1116 insoluble particles : a theoretical framework, *Atmos. Chem. Phys.*, (7), 6175–6180, 2007.
- 1117 Stratmann, F., Bilde, M., Dusek, U., Frank, G. P., Hennig, T., Henning, S., Kiendler-Scharr, a.,
1118 Kiselev, a., Kristensson, a., Lieberwirth, I., Mentel, T. F., Pöschl, U., Rose, D., Schneider, J.,
1119 Snider, J. R., Tillmann, R., Walter, S. and Wex, H.: Examination of laboratory-generated coated
1120 soot particles: An overview of the LACIS Experiment in November (LEXNo) campaign, *J.*
1121 *Geophys. Res.*, 115(D11), D11203, doi:10.1029/2009JD012628, 2010.

- 1122 Sugio, S., Kashima, a, Mochizuki, S., Noda, M. and Kobayashi, K.: Crystal structure of human
1123 serum albumin at 2.5 Å resolution., *Protein Eng.*, 12(6), 439–46 [online] Available from:
1124 <http://www.ncbi.nlm.nih.gov/pubmed/10388840>, 1999.
- 1125 Twomey, S.: Pollution and the planetary albedo, *Atmos. Environ.*, 8, 1251–1256, 1974.
- 1126 Virtanen, A., Ristimäki, J. and Keskinen, J.: Method for measuring effective density and fractal
1127 dimension of aerosol agglomerates, *Aerosol Sci. Technol.*, 38(5), 437–446,
1128 doi:10.1080/02786820490445155, 2004.
- 1129
- 1130

1131 Table 1: Thermodynamic properties of components used in this study.

	Molar mass (g/mol)	Density (g/cm³)	Solubility in water (Mass%)	κ
(NH₄)₂SO₄	132.14 ^a	1.77 ^a	43.3 ^a	0.61 ^e
Sucrose	342.3 ^a	1.58 ^a	67.1 ^a	0.084 ^f
BSA	66500 ^b	1.362 ^b	60 ^d	0.013 ^g
SiO₂	60.08 ^a	2.16 ^c	-	-

1132 ^a Haynes et al. (2013)

1133 ^b Mikhailov et al. (2004)

1134 ^c Grayson (1985)

1135 ^d Shiraiwa et al. (2011)

1136 ^e Petters and Kreidenweis (2007)

1137 ^f Ruehl et al. (2010)

1138 ^g This work

1139

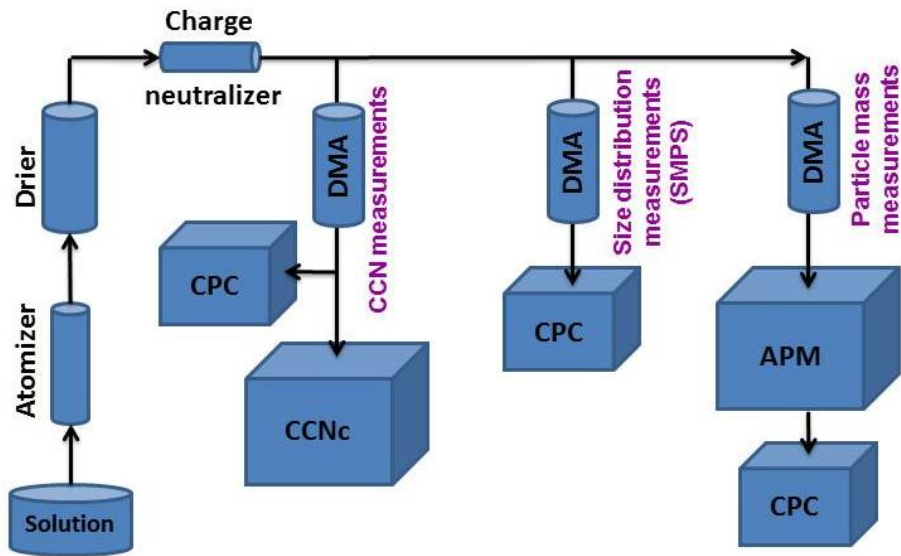
1140 Table 2: The total soluble fraction of the solute masses in the bulk mixtures, the fraction of total
 1141 soluble mass mixed with silica, the average soluble mass fraction of the mixed particles
 1142 (calculated from particle size distributions, see text for details).

Soluble mass fraction in the bulk mixture (%)	Fraction of total soluble mass mixed with silica (%)			Total soluble mass fraction in the mixed particles (%)		
	Silica+ (NH ₄) ₂ SO ₄	Silica+ sucrose	Silica+ BSA	Silica+ (NH ₄) ₂ SO ₄	Silica+ sucrose	Silica+ BSA
25	92	98	87	23.4	24.6	22.5
10	88	99	99	8.9	9.9	9.9
5	87	99	~100	4.4	4.9	~5

1143

1144

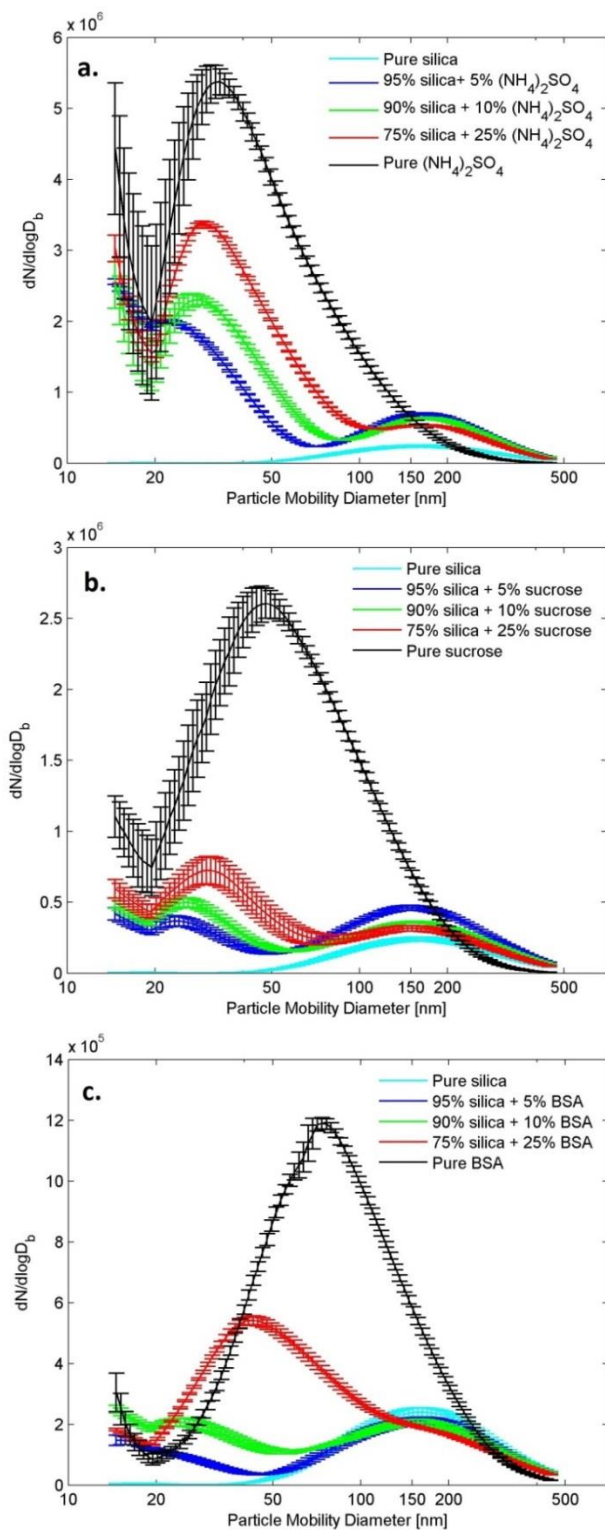
1145



1146

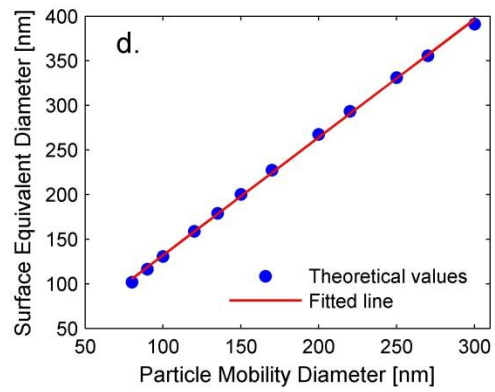
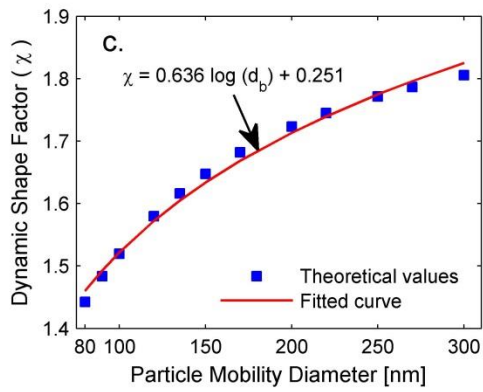
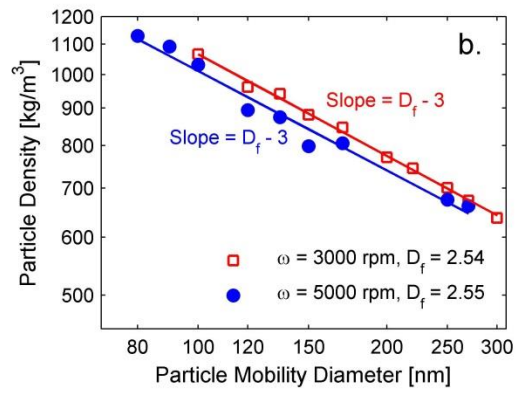
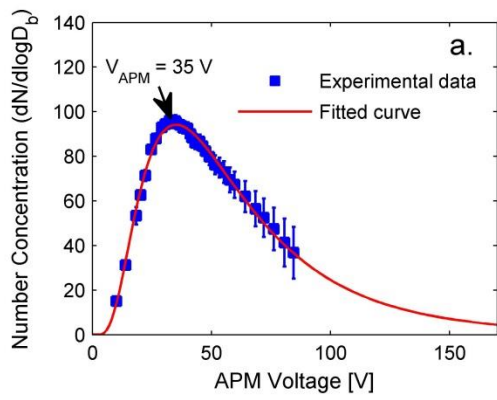
1147 Fig. 1: Schematic of the experimental set up and three types of measurements: CCN activity
1148 measurements, size distribution measurements by SMPS and particle mass analyzing by APM.

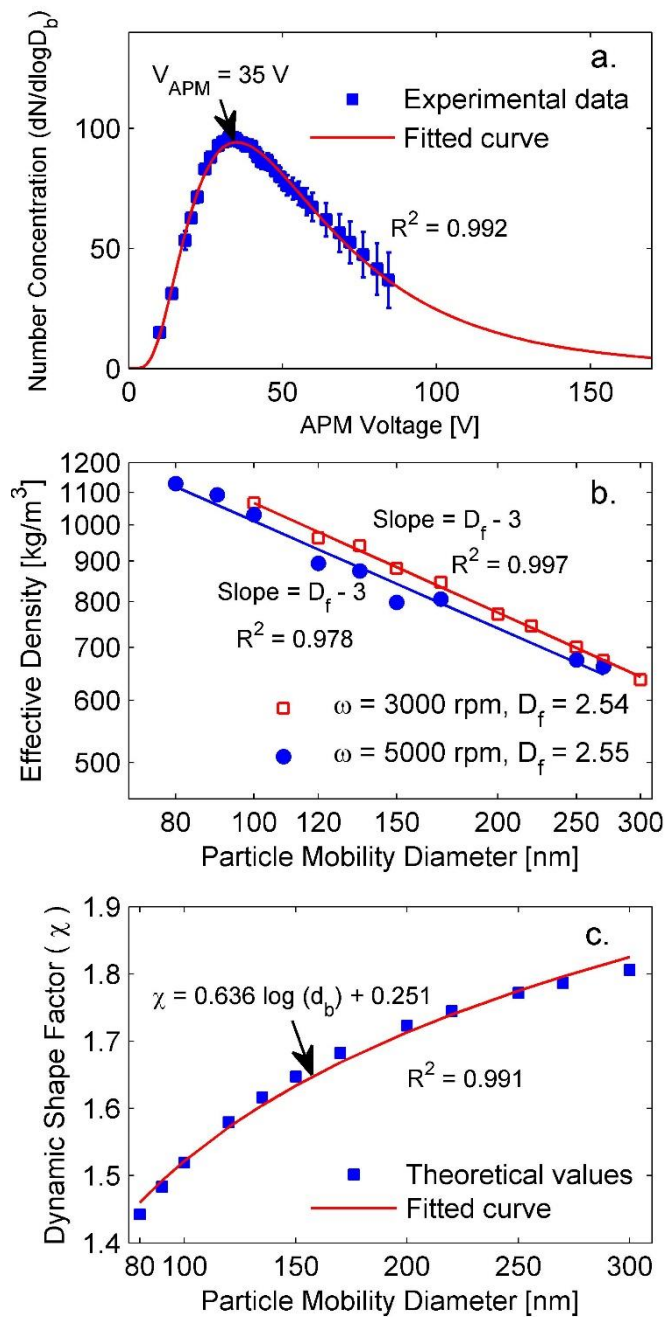
1149



1150

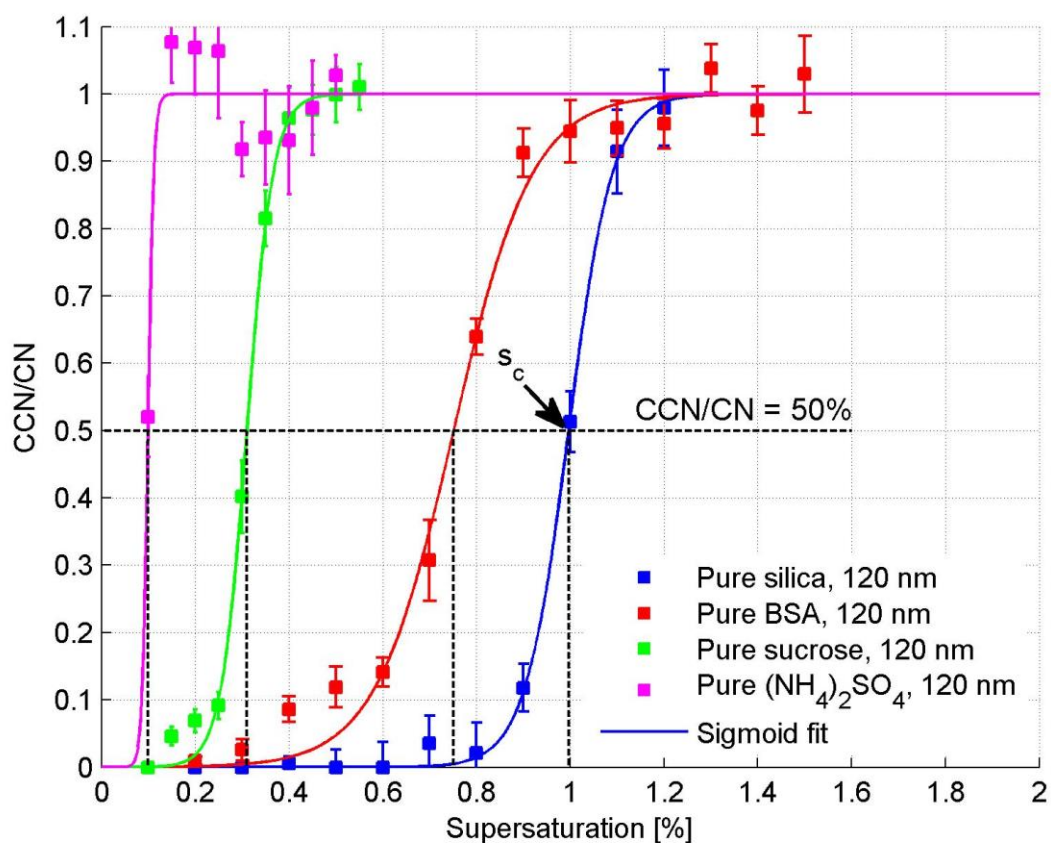
1151 Fig. 2: Average particle number size distributions (SMPS) for silica particles mixed with **(a)**
 1152 $(\text{NH}_4)_2\text{SO}_4$, **(b)** sucrose and **(c)** BSA. Each average size distribution is based on at least 70
 1153 individual size distributions, and the error bars represent the standard deviation of the
 1154 measurements.



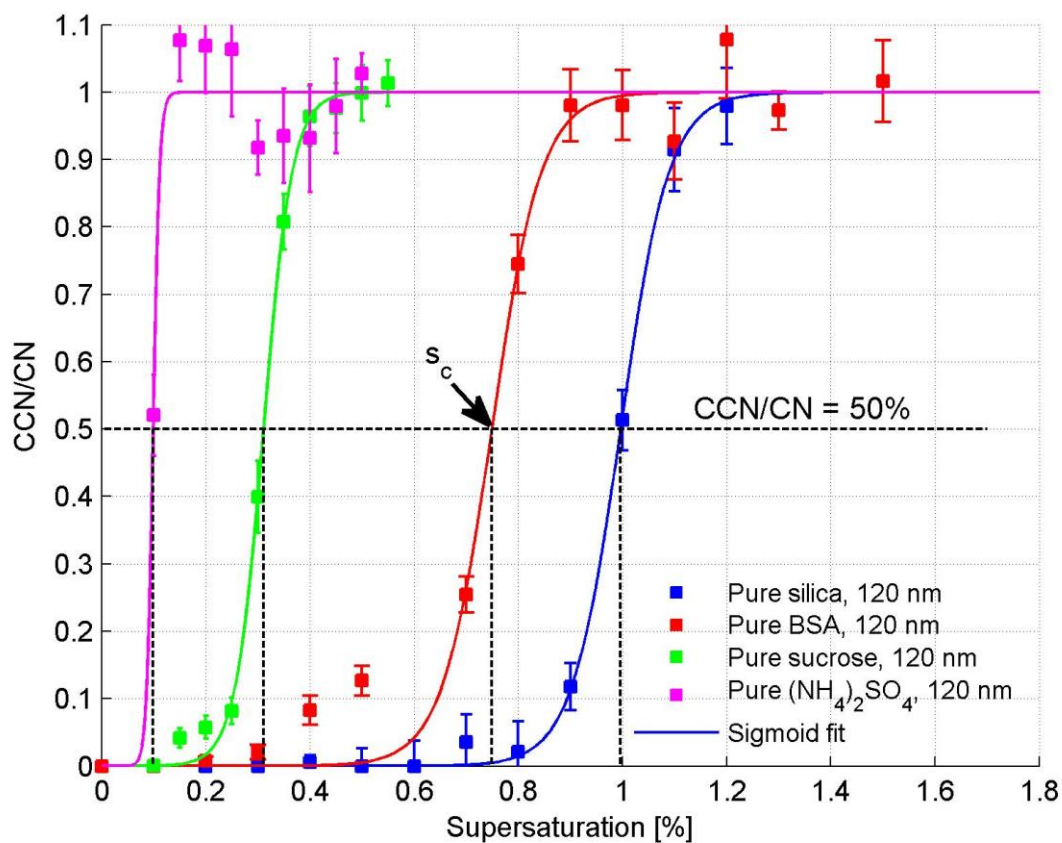


1156

1157 Fig. 3: **(a)** Average number concentration of 100 nm (mobility size) pure silica particles
 1158 downstream the APM and at a rotation speed of the APM of 3000 rpm. The number
 1159 concentrations were averaged over one minute for each APM voltage, and the error bars
 1160 represent the standard deviation of about 60 measurements recorded under the same conditions.
 1161 **(b)** Density-Effective density of silica particles for different mobility diameters and two
 1162 different rotation speeds of the APM (3000 and 5000 rpm). The fitted fractal dimensions are
 1163 2.54 and 2.55, respectively. **(c)** Dynamic-Mass-based shape factor versus electrical mobility
 1164 diameter for silica particles, ~~**(d)** Theoretical surface equivalent diameter against mobility~~
 1165 ~~diameter of the silica particles.~~



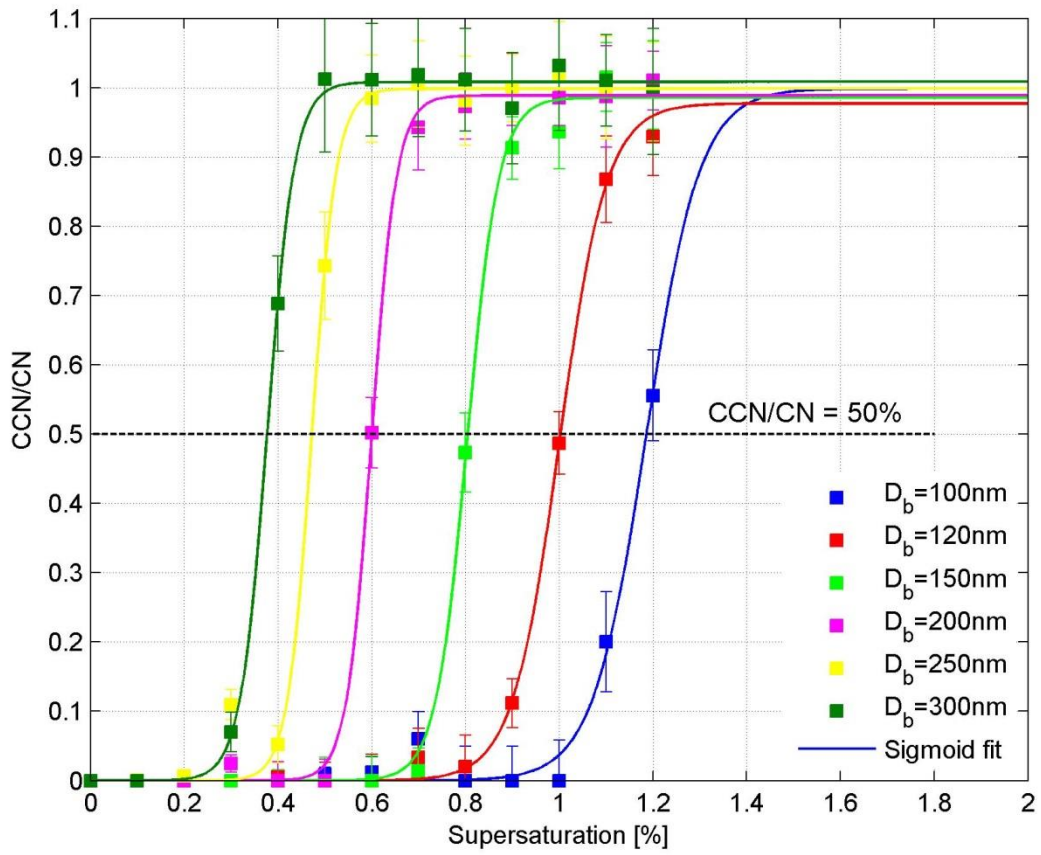
1167



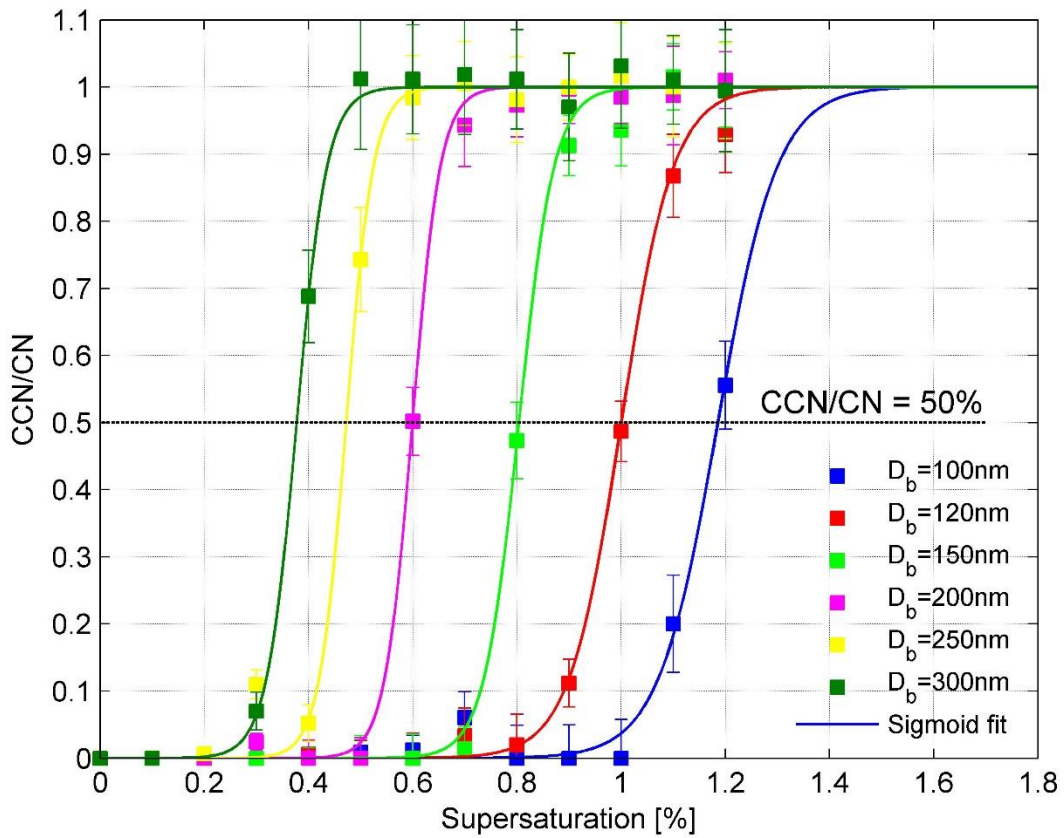
1168

1169 Fig. 4: The average activation ratio of pure soluble or insoluble particles with the mobility
1170 diameter of 120 nm at different supersaturations. Error bars represent the standard deviation
1171 of the activation efficiency of about 20 measurements corresponding to each supersaturation
1172 of the instrument. Critical supersaturation s_c is defined as the point where the activation ratio
1173 is equal to 50%.

1174



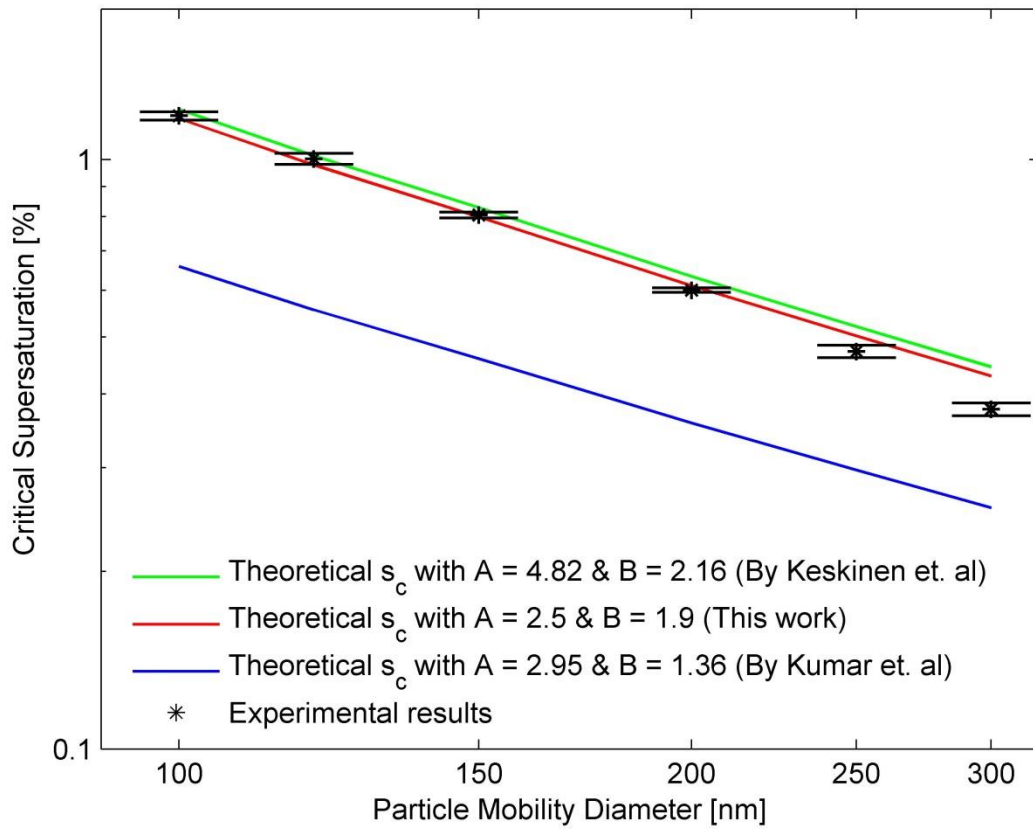
1175



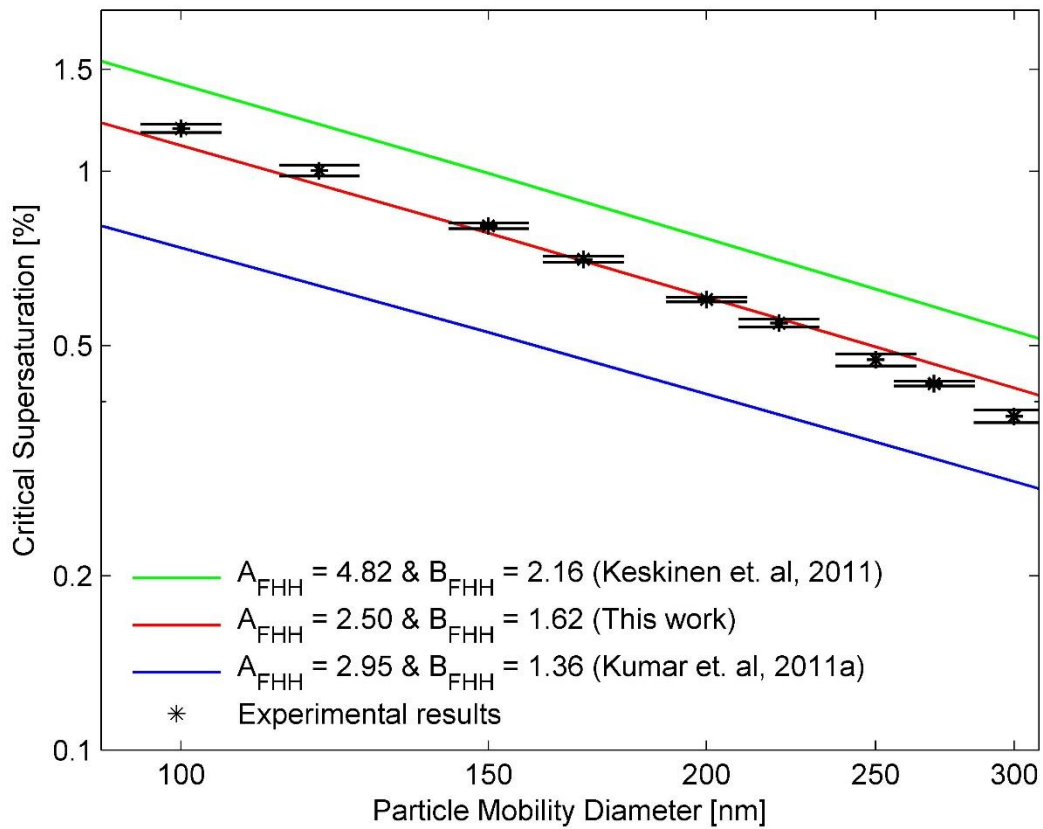
1176

1177 Fig. 5: The average activation ratio versus supersaturation for different mobility diameters of
1178 silica particles. Error bars represent the standard deviation of the measured activation efficiency
1179 as a result of about 20 measurements corresponding to each supersaturation of the instrument.

1180



1181

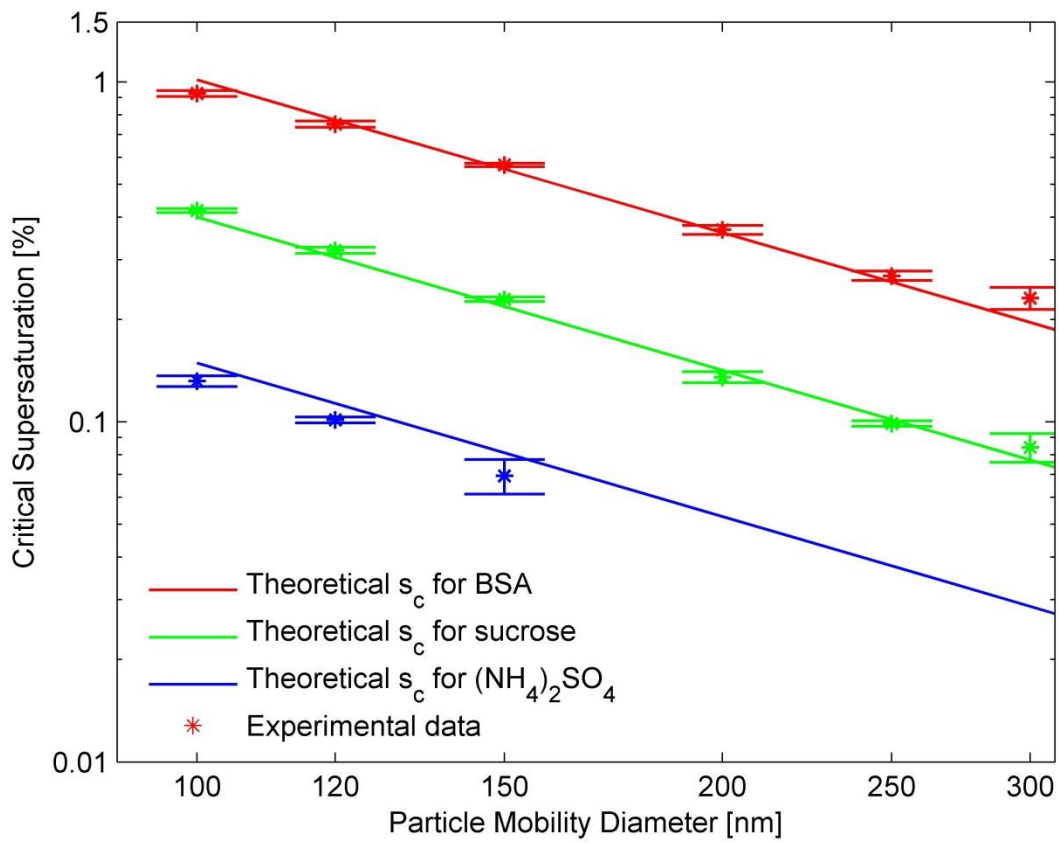


1182

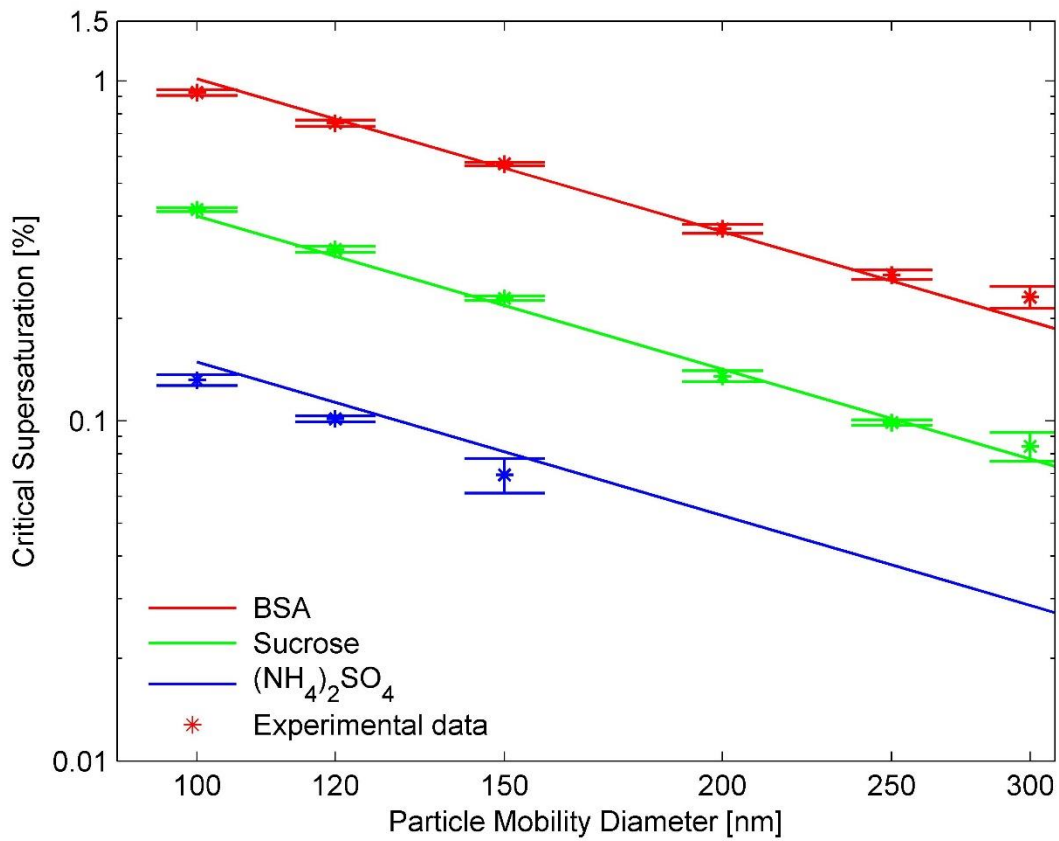
1183 Fig. 6: Critical supersaturations against activation mobility diameter of pure silica particles with
1184 different FHH adsorption isotherm parameters from different studies compared to experimental
1185 results. Error bars represent the minimum vs. maximum values of supersaturation to estimate
1186 the s_c corresponding to each d_b .

1187

1188



1189



1190

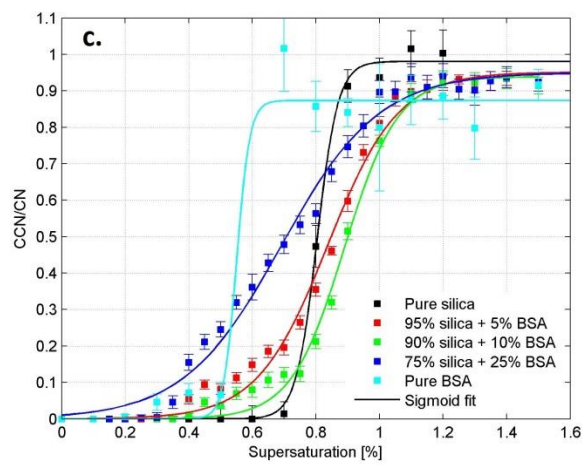
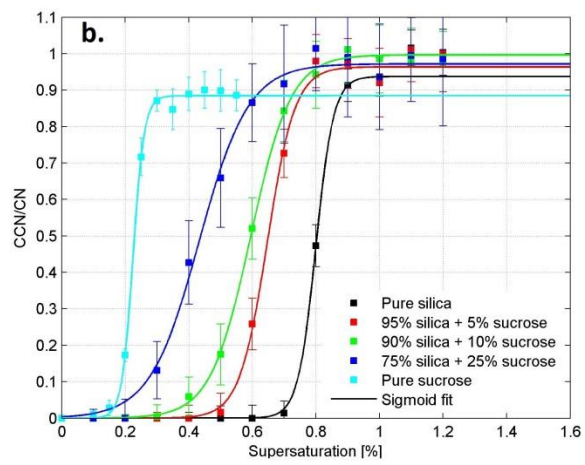
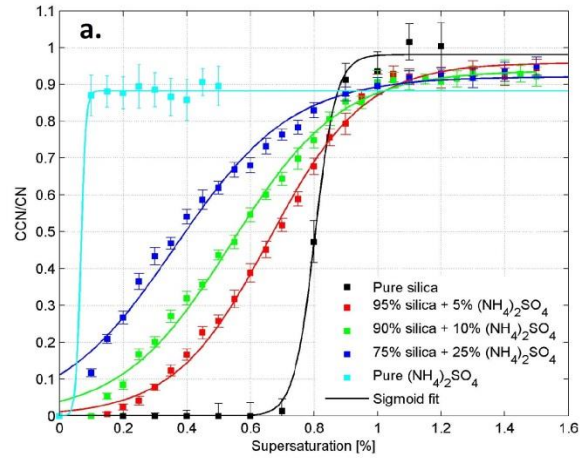
1191 Fig. 7: Experimental and theoretical critical supersaturations of pure $(\text{NH}_4)_2\text{SO}_4$, sucrose and
1192 BSA particles for different mobility diameters based on κ -Köhler theory. Error bars represent
1193 the minimum vs. maximum values of supersaturation to estimate the s_c corresponding to each
1194 d_b .

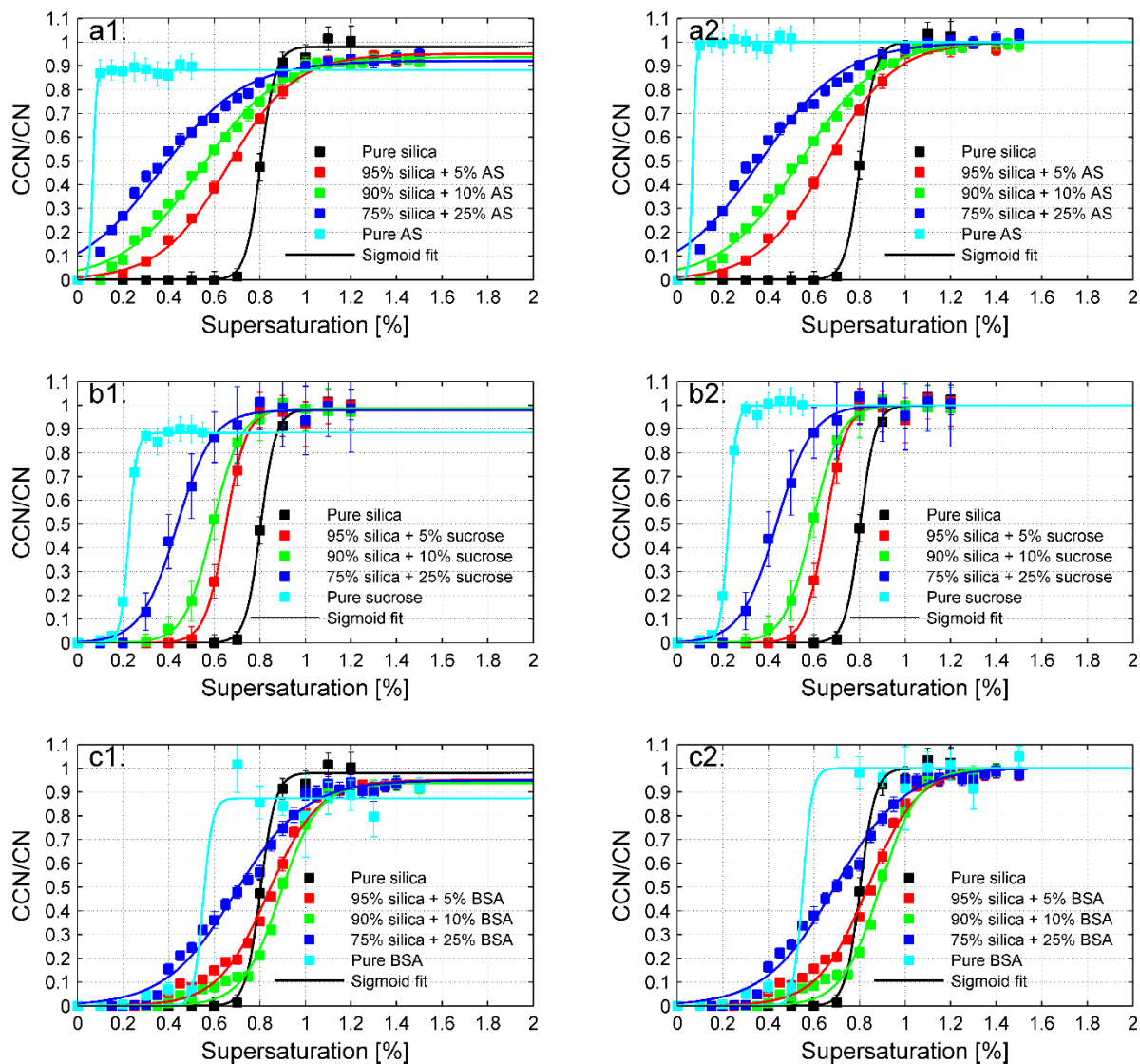
1195

1196

1197

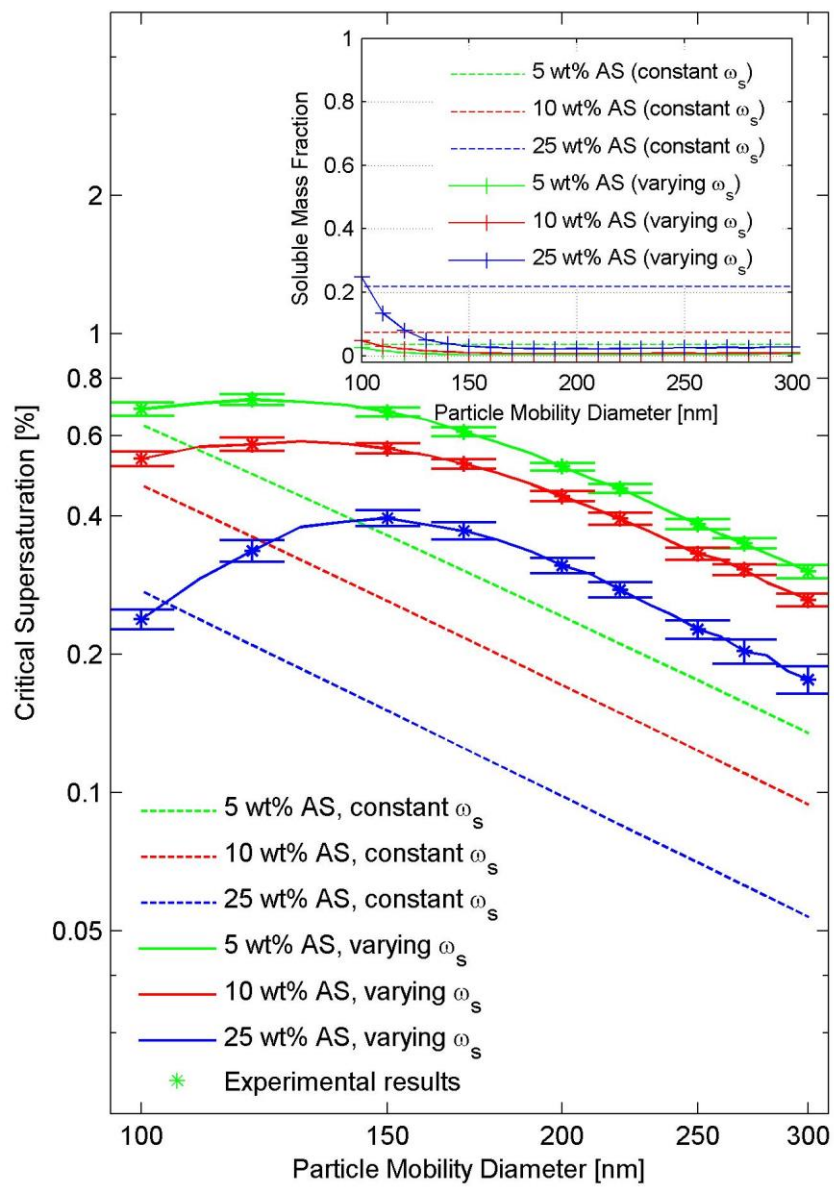
1198

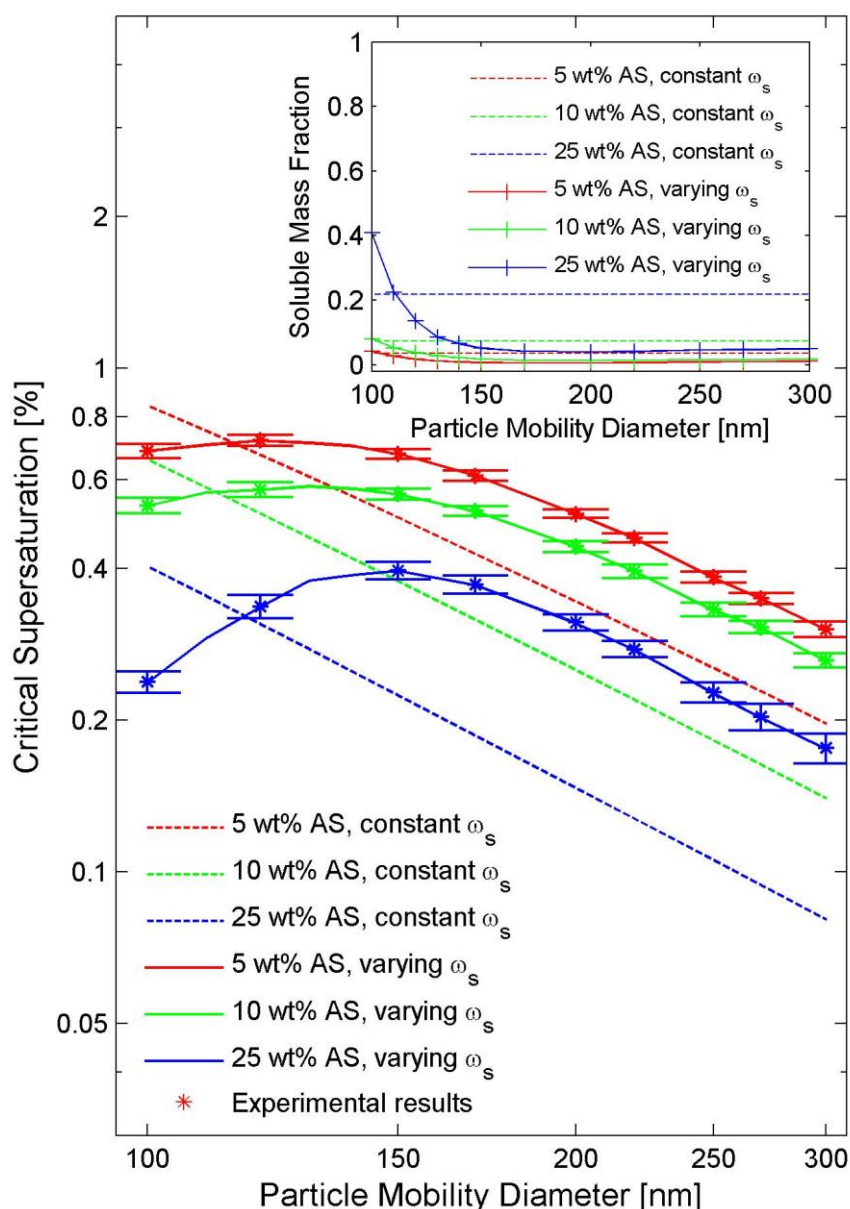




1200

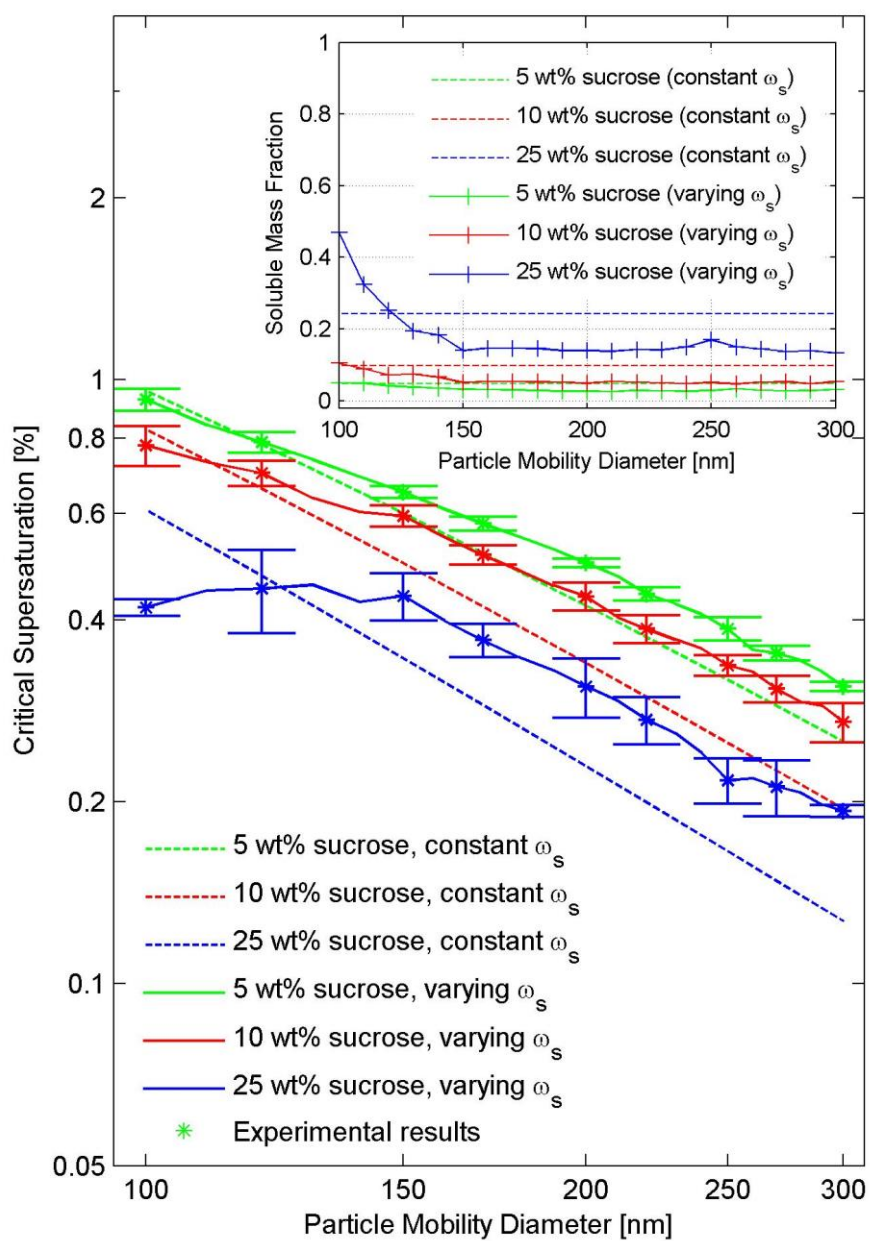
1201 Fig. 8: (a) Activation ratio curves for different supersaturations of silica + $(\text{NH}_4)_2\text{SO}_4$ particles
 1202 of 150 nm mobility diameter, (b) Activation ratio curves for different supersaturations of silica
 1203 + sucrose particles of 150 nm mobility diameter, (c) Activation ratio curves for different
 1204 supersaturations of silica + BSA particles of 150 nm mobility diameter. [The activation curves](#)
 1205 [on the left side \(subplots a1-c1\) represent the unnormalized data, while the activation curves on](#)
 1206 [the right side \(subplots a2-c2\) show the normalized ones.](#) Error bars represent the standard
 1207 deviation of the measured activation efficiency as a result of about 20 measurements
 1208 corresponding to each supersaturation of the instrument.

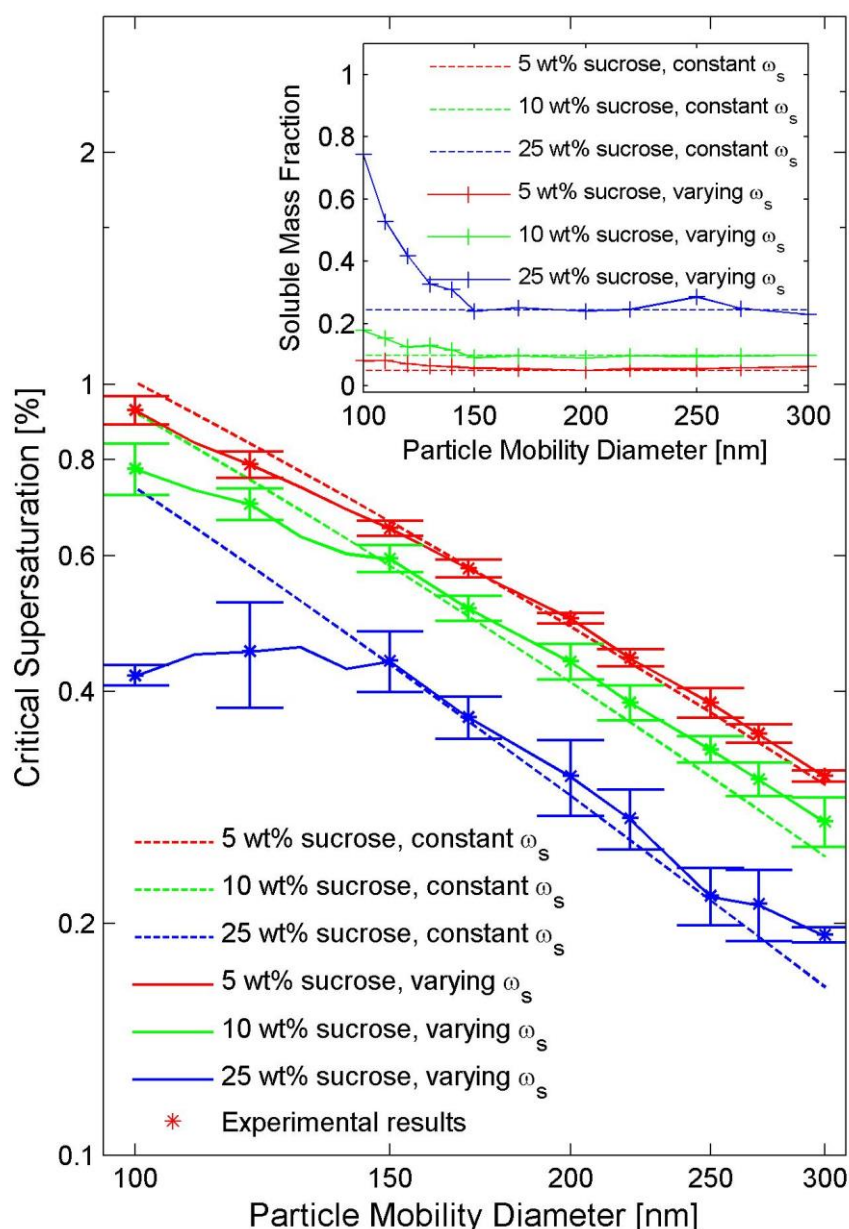




1210

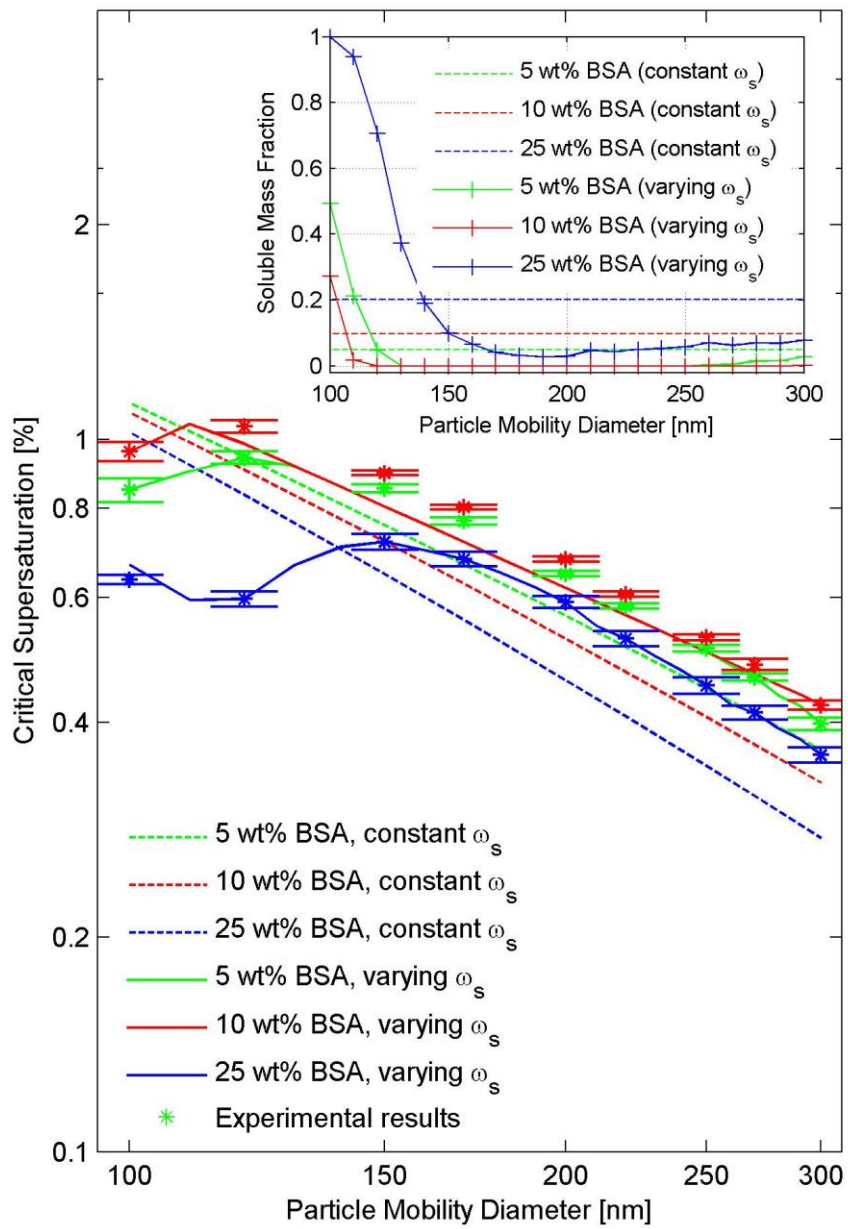
1211 Fig. 9: Experimental and theoretical critical supersaturations for mixed silica + $(\text{NH}_4)_2\text{SO}_4$ (AS)
 1212 particles for different particle mobility diameters using [theshell-and-core model by Kumar et](#)
 1213 [al. \(2011b\)](#). Dashed lines represent calculated critical supersaturations based on an assumption
 1214 of constant soluble mass fractions (ω_s) with changing diameter and solid lines show the critical
 1215 supersaturations based on the size-dependent soluble mass fractions. Error bars represent the
 1216 minimum vs. maximum values of supersaturation to estimate the s_c corresponding to each
 1217 mobility diameter. The inset represents assumed constant soluble mass fractions as well as size-
 1218 dependent ones corresponding to the 50% points in the CCN/CN curves for different size vs.
 1219 supersaturation pairs of mixed silica + $(\text{NH}_4)_2\text{SO}_4$ particles.

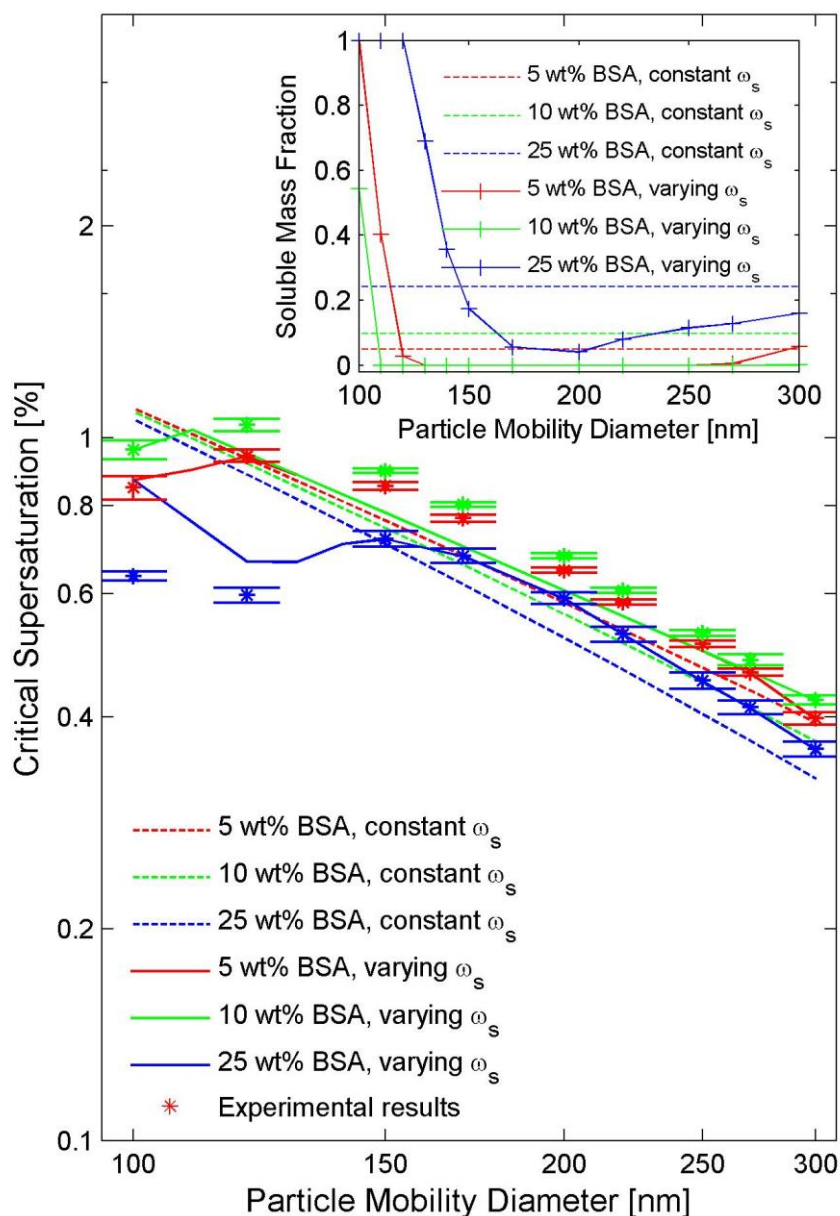




1221

1222 Fig. 10: Experimental and theoretical critical supersaturations for mixed silica + sucrose
 1223 particles for different particle mobility diameters using [shell-and-core](#) model [by Kumar et](#)
 1224 [al. \(2011b\)](#). Dashed lines represent calculated critical supersaturations based on an assumption
 1225 of constant soluble mass fractions (ω_s) with changing diameter and solid lines show the critical
 1226 supersaturations based on the size-dependent soluble mass fractions. Error bars represent the
 1227 minimum vs. maximum values of supersaturation to estimate the s_c corresponding to each
 1228 mobility diameter. The inset represents assumed constant soluble mass fractions as well as size-
 1229 dependent ones corresponding to the 50% points in the CCN/CN curves for different size vs.
 1230 supersaturation pairs of mixed silica + sucrose particles.

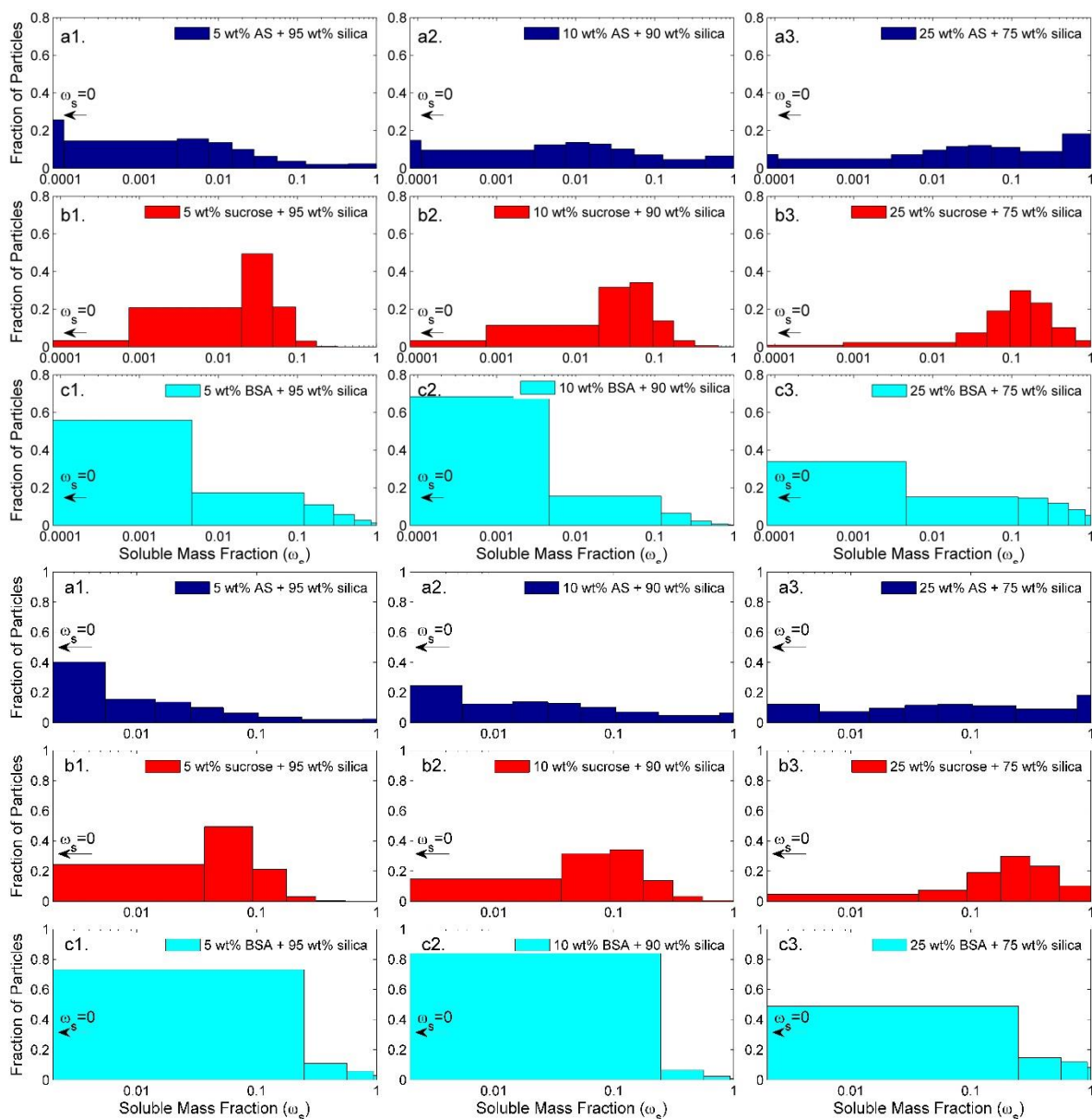




1232

1233 Fig. 11: Experimental and theoretical critical supersaturations for mixed silica + BSA particles
 1234 for different particle mobility diameters using [shell-and-core](#) model [by Kumar et al. \(2011b\)](#).
 1235 Dashed lines represent calculated critical supersaturations based on an assumption of constant
 1236 soluble mass fractions (ω_s) with changing diameter and solid lines show the critical
 1237 supersaturations based on the size-dependent soluble mass fractions. Error bars represent the
 1238 minimum vs. maximum values of supersaturation to estimate the s_c corresponding to each
 1239 mobility diameter. The inset represents assumed constant soluble mass fractions as well as size-
 1240 dependent ones corresponding to the 50% points in the CCN/CN curves for different size vs.
 1241 supersaturation pairs of mixed silica + BSA particles.

1242



1243

1244 Fig. 12: The distribution of soluble material on 150 nm (mobility diameter) particles in the
 1245 mixed particles made of (a1-3) silica + $(\text{NH}_4)_2\text{SO}_4$ (AS), (b1-3) silica + sucrose, (c1-3) silica +
 1246 BSA. Note that the smallest solubility bin extends down to zero, i.e. particles consisting of pure
 1247 silica.